

# Statistical characteristics of observed Ly- $\alpha$ forest and the shape of initial power spectrum

M. Demiański<sup>1,2</sup>, A.G. Doroshkevich<sup>3,4</sup> & V. Turchaninov<sup>4</sup>

<sup>1</sup>*Institute of Theoretical Physics, University of Warsaw, 00-681 Warsaw, Poland*

<sup>2</sup>*Department of Astronomy, Williams College, Williamstown, MA 01267, USA*

<sup>3</sup>*Theoretical Astrophysics Center, Juliane Maries Vej 30, DK-2100 Copenhagen Ø, Denmark*

<sup>4</sup>*Keldysh Institute of Applied Mathematics, Russian Academy of Sciences, 125047 Moscow, Russia*

Accepted ..., Received ..., in original form ...

## ABSTRACT

Properties of  $\sim 5000$  observed Ly- $\alpha$  absorbers are investigated using the model of formation and evolution of DM structure elements based on the Zel'dovich theory. This model is generally consistent with simulations of absorbers formation, accurately describes the Large Scale Structure observed in the galaxy distribution at small redshifts and emphasizes the generic similarity of the LSS and absorbers.

The simple physical model of absorbers asserts that they are composed of DM and gaseous matter and it allows us to estimate the column density and overdensity of DM and gaseous components and the entropy of the gas trapped within the DM potential wells. The parameters of DM component are found to be consistent with theoretical expectations for the Gaussian initial perturbations with the WDM-like power spectrum. We demonstrate the influence of the main physical factors responsible for the absorbers evolution.

The analysis of redshift distribution of absorbers confirms the self consistence of the assumed physical model and allows to estimate the shape of the initial power spectrum at small scales what in turn restricts the mass of dominant fraction of DM particles to  $M_{DM} \approx 0.6 - 2$  keV. Our results verify the redshift variations of intensity of the UV background by about 4 – 6 times and indicate that, perhaps, the available observations underestimate the intensity of this background.

**Key words:** cosmology: large-scale structure of the Universe — quasars: absorption: general — surveys.

## 1 INTRODUCTION

One of the most perspective methods to study the processes responsible for the formation and evolution of the structure of the Universe is the analysis of properties of absorbers observed in spectra of the farthest quasars. The great potential of such investigations was discussed already in Oort (1981, 1984) just after Sargent et al. (1980) established intergalactic nature of the Ly- $\alpha$  forest. The available Keck and VLT high resolution observations of the forest provide a reasonable database and allow to apply statistical methods for such investigations.

The essential progress achieved recently through numerous high resolution simulations of absorber formation and evolution confirms that this process is closely connected with the initial power spectrum of perturbations. These results allow us to consider the properties of absorbers in the context of nonlinear theory of gravitational instability (Zel'dovich

1970; Shandarin & Zel'dovich 1988) and to use the statistical description of their properties (Demiański & Doroshkevich 1999, 2002; hereafter DD99 & DD02; Demiański et al. 2000). This approach was already discussed in Demiański, Doroshkevich & Turchaninov (2001 a,b, hereafter Paper I & Paper II). Here we improve this analysis by using the richer and more refined sample of  $\sim 5000$  observed absorbers and more refined model of absorbers.

This approach uses more traditional methods of investigation of properties of discrete absorbers rather than associating them with a continuous non-linear line-of-sight density field (see, e.g., Weinberg et al. 1998; Croft et al. 2001). It allows to reach more clarity in the description of formation and evolution of structure, to reveal its strong dependence on the initial power spectrum and to compare the evolution of observed absorbers and invisible DM component.

Some results of the statistical description derived in DD99, DD02 and Demiański et al. 2000 for the CDM-like

initial power spectrum are consistent with characteristics of the Large Scale Structure found for simulated and observed matter distribution at small redshifts (Demiański et al. 2000; Doroshkevich, Tucker & Allam 2002). Here we use this approach for the analysis and interpretation of the absorbers observed at large redshifts. We show that the basic observed characteristics of Ly- $\alpha$  absorbers are also successfully described in the framework of this theoretical model.

In this model several factors are influencing the evolution of structure which can be outlined as a random formation and merging of Zel'dovich pancakes, their transverse expansion and/or compression, and their final transformation into high density clouds and filaments. Later on, the hierarchical merging of pancakes, filaments and clouds forms rich walls observed at small redshifts. Main steps of this evolution are driven by the initial power spectrum. The approach used here makes it possible to discriminate between the action of these factors and to separate approximately several subpopulations of absorbers that illustrate these evolutionary stages.

The composition and spatial distribution of observed absorbers is complicated and at low redshifts a significant number of stronger Ly- $\alpha$  lines and metal systems is associated with galaxies (Bergeron et al. 1992; Lanzetta et al. 1995; Tytler 1995; Le Brune et al. 1996). However as was recently shown by Penton, Stock and Shull (2002), even at small redshifts some absorbers are associated with galaxy filaments while others are found within galaxy voids.

These results suggest that the population of weaker absorbers dominating at higher redshifts can be associated with the population of weaker structure elements formed by the non luminous baryonic and DM components in extended low density regions. In turn, the relatively homogeneous spatial distribution of absorbers implies a more homogeneous spatial distribution of both DM and baryonic components as compared with the observed distribution of the luminous matter.

Some progress in the interpretation of the redshift distribution of absorbers was already achieved in Paper I. Now we use a more refined theoretical model which allows to estimate independently the DM characteristics of the sample under investigation, to reveal essential redshift variations of the UV background and to link the fitted parameters with spectral moments of the initial power spectrum. In turn, these results allow to test the adopted physical model and to estimate the mass of particles dominating DM.

This theory cannot yet describe in details the process of relaxation of compressed matter, the disruption of structure elements due to the gravitational instability of compressed DM, and the distribution of neutral hydrogen across DM pancakes. Therefore, in this paper several numerical factors remain undetermined and they could be restricted by some other estimates of properties of DM pancakes.

This analysis must be supplemented by application of the discussed here methods to simulations which take simultaneously into account the impact of many important factors and provide unified picture of the process of absorber formation and evolution. But so far such simulations can be performed only in small boxes what restricts their representativity, introduces artificial cutoffs in the power spectrum and complicates the quantitative description of structure evolution.

Comparison of results obtained in Paper I and Paper II and in this paper demonstrates that the quality and representativity of the sample of observed absorbers is very important for the reconstruction of processes of structure formation at high redshifts. In this paper we use the sample of  $\sim 5000$  absorbers at  $1.7 \leq z \leq 3.5 - 4$  but unfortunately some of our results are based on the poor statistics. Further progress can be achieved with richer samples covering the range of redshifts at least up to  $z \sim 4.5 - 5$ . The observational evidence of the reheating of the Universe at  $z \approx 6$  (Djorgovski et al 2001; Fan et al. 2001) makes it extremely important to perform a complex investigation of the earlier period of structure evolution at redshifts  $z \sim 4 - 6$ .

This paper is organized as follows. The theoretical model of the structure evolution is discussed in Sec. 2. In Sec. 3 the observational databases used in our analysis are presented. The results of statistical analysis are given in Secs. 4 – 6. Discussion and conclusion can be found in Sec. 7.

## 2 MODEL OF ABSORBERS FORMATION AND EVOLUTION

The main observational characteristics of absorption lines are the redshift,  $z_{abs}$ , the column density of neutral hydrogen,  $N_H$ , and the Doppler parameter,  $b$ , while the theoretical description of structure formation and evolution is dealing with the mean linear number density of DM absorbers,  $n_{abs}(z)$ , temperature,  $T$ , overdensity and entropy of the gaseous component, and with the ionization degree of hydrogen. To connect these theoretical and observed parameters a physical model of absorbers formation and evolution is required.

Many such models were proposed and discussed during the last twenty years (see references in Rauch 1998, and in Paper I and Paper II). However, to describe the properties of the new wider and refined sample of observed absorbers it is necessary to develop a more detailed physical model of absorbers as well. Our model includes some ideas discussed already in earlier publications.

### 2.1 Physical model of absorbers.

In this paper we assume that:

(i) The DM distribution forms an interconnected structure of sheets (Zel'dovich pancakes) and filaments, their main parameters are approximately described by the Zel'dovich theory of gravitational instability applied to CDM or WDM initial power spectrum (DD99; DD02; Demiański et al. 2000). The majority of DM pancakes are partly relaxed, long-lived, and their properties vary due to expansion and compression in the transverse directions.

(ii) Gas is trapped in the gravitational potential wells formed by the DM distribution. The gas temperature and the observed Doppler parameter,  $b$ , trace the depth of the DM potential wells.

(iii) For a given temperature, the gas density within the wells is determined by the gas entropy created during the previous evolution. The gas entropy is changing, mainly, due to shocks heating in the course of merging of pancakes, bulk heating produced by local sources and due to radiative cooling.

(iv) The gas is ionized by the UV background and for the majority of absorbers ionization equilibrium is assumed.

(v) The observed properties of absorbers are changing because of merging, transversal compression and/or expansion and disruption of DM pancakes. The bulk heating and radiative cooling leads to slow drift of the entropy and density of the trapped gas. Variations of the intensity and the spectrum of the ionizing UV radiation field produce moderate discrepancies between the observed and expected properties of absorbers.

(vi) In this simple model we identify the velocity dispersion of DM component compressed within pancakes with the temperature of hydrogen and the Doppler parameter  $b$  of absorbers. We consider the possible macroscopic motions within pancakes as subsonic and assume that they cannot essentially distort the measured Doppler parameter.

As compared with the model discussed in Paper II, here we take into account more accurately the evolution of pancakes after their formation.

The formation of DM pancakes as an inevitable first step of evolution of small perturbations was firmly established both by theoretical considerations (Zel'dovich 1970; Shandarin & Zel'dovich 1989) and numerically (Shandarin et al. 1995). Both theoretical analysis and simulations show the successive transformation of sheet-like elements into filamentary-like ones and, at the same time, the merging of both sheet-like and filamentary elements into richer walls. Such continuous transformation of structure goes on all the time. These processes imply the existence of a complicated time-dependent internal structure of high density elements and, in particular, the essential arbitrariness in discrimination of such elements into filaments and sheets.

Our approximate consideration cannot be applied to objects for which the gravitational potential and the gas temperature along the line of sight depend essentially on the matter distribution across this line. In this paper we use the term 'pancake' to denote structure elements with relatively small gradient of properties across the line of sight. With such a criterion, the anisotropic halo of filaments and clouds can also be considered as 'pancake-like'.

The subpopulation of weaker absorbers also contains "artificial" caustics (McGill 1990) and absorbers identified with slowly expanding underdense regions (Bi & Davidsen 1997; Zhang et al. 1998; Davé et al. 1999). Such absorbers produce a short lived noise, which is stronger at higher redshifts  $z \geq 3$ . Fortunately, fraction of such absorbers does not exceed 10% of the observed sample and they cannot significantly distort our final estimates.

In this paper we consider the spatially flat  $\Lambda$ CDM model of the Universe with the Hubble parameter and mean density

$$H^2 = H_0^2 \Omega_m (1+z)^3 [1 + \Omega_\Lambda / \Omega_m (1+z)^{-3}], \quad (1)$$

$$\langle \rho_m(z) \rangle = \frac{3H_0^2}{8\pi G} \Omega_m (1+z)^3, \quad H_0 = 100h \text{ km/s/Mpc}.$$

Here  $\Omega_m$  &  $\Omega_\Lambda$  are dimensionless matter density and the cosmological term,  $\Omega_m + \Omega_\Lambda = 1$ , and  $h$  is the dimensionless Hubble constant.

## 2.2 Properties of the homogeneously distributed hydrogen

The properties of compressed gas can be suitably related to better known parameters of homogeneously distributed gas, which were described in many papers (see, e.g., Ikeuchi & Ostriker 1986). For example, the baryonic density and the temperature can be taken as

$$\langle n_b(z) \rangle = 1.2 \cdot 10^{-5} \Omega_b h^2 (1+z)^3 \text{ cm}^{-3}, \quad (2)$$

$$T_{bg} \approx 1.6 \cdot 10^4 K, \quad b_{bg} = \sqrt{\frac{2k_B T_{bg}}{m_H}} \approx 16 \text{ km/s}.$$

Here  $\Omega_b$  is the dimensionless mean density of baryons,  $k_B$  is the Boltzmann's constant,  $b_{bg}$  is the Doppler parameter of gas, and  $m_H$  is the mass of the hydrogen atom.

Under the assumption of ionization equilibrium of the gas

$$\alpha_{rec} n_b^2 \approx n_H \Gamma_\gamma, \quad (3)$$

and for the recombination coefficient

$$\alpha_{rec}(T) \approx 4 \cdot 10^{-13} \left( \frac{10^4 K}{T} \right)^{3/4} \frac{\text{cm}^3}{s},$$

(Black, 1981), the fraction of neutral hydrogen is

$$x_{bg} = n_H / n_b = \langle n_b(z) \rangle \alpha_{rec}(T_{bg}) \Gamma_\gamma^{-1} = x_0 (1+z)^3, \quad (4)$$

$$x_0 \approx 6.7 \cdot 10^{-8} \frac{\Omega_b h^2}{0.02} \frac{1}{\Gamma_{12}}, \quad \Gamma_\gamma = 10^{-12} s^{-1} \Gamma_{12},$$

where  $\Gamma_\gamma$  characterizes the rate of ionization by the UV background. For the standard power law spectrum of radiation

$$J(\nu) = J_{21} \cdot 10^{-21} \left( \frac{\nu_H}{\nu} \right)^{\alpha_\gamma} \text{ erg s}^{-1} \text{ cm}^{-2} \text{ sr}^{-1} \text{ Hz}^{-1},$$

we get that

$$\Gamma_{12} = 12.6 J_{21} (3 + \alpha_\gamma)^{-1}.$$

The gas entropy can be characterized by the function

$$F_{bg} = \frac{T_{bg}}{\langle n_b \rangle^{2/3}} = \frac{F_0}{(1+z)^2} \approx \frac{36 \text{ keV} \cdot \text{cm}^2}{(1+z)^2} \left( \frac{0.02}{\Omega_b h^2} \right)^{2/3}. \quad (5)$$

## 2.3 Parameters of absorbers

In this section we introduce main relations between theoretical and observed characteristics of pancakes based on the physical model discussed in Sec. 2.1. The most important characteristics of DM pancakes are presented (without proofs) as a basis for further analysis.

### 2.3.1 Characteristics of DM component

The fundamental characteristics of DM pancakes are the dimensionless Lagrangian thickness,  $q$ , and the DM column (or surface) density,  $\mu$ :

$$\mu \approx \frac{\langle \rho_m(z) \rangle l_v q}{(1+z)} = \frac{3H_0^2}{8\pi G} l_v \Omega_m (1+z)^2 q, \quad (6)$$

$$l_v \approx \frac{6.6}{h \Omega_m} h^{-1} \text{ Mpc} = 33.8 h^{-1} \text{ Mpc} \frac{0.3}{\Omega_m} \frac{0.65}{h},$$

where  $l_v$  is the coherent length of initial velocity field (DD99; DD02),  $\langle \rho_m(z) \rangle \propto \Omega_m(1+z)^3$ . The Lagrangian thickness of pancake,  $l_v q$ , is defined as the unperturbed distance at redshift  $z = 0$  between positions of DM particles bounding the pancake. The actual thickness of pancake is

$$\Delta r = \mu \langle \rho_m \rangle^{-1} \delta^{-1} = l_v q (1+z)^{-1} \delta^{-1}. \quad (7)$$

Here  $\delta$  is the mean overdensity of pancake above the mean background density.

The expected probability distribution function (PDF) for the Lagrangian thickness of a pancake,  $q$ , can be written (DD99, DD02) as

$$N_q dq \approx \frac{2}{\sqrt{\pi}} \cdot e^{-\xi} \frac{\text{erf}(\sqrt{\xi})}{\sqrt{\xi}} \left( \frac{q^2}{q^2 + q_0^2} \right)^{3/4} d\xi, \quad \xi = \frac{q}{8\tau^2}, \quad (8)$$

$$< \xi > = 0.5 + 1/\pi \approx 0.82, \quad \tau(z) = \tau_0 B(z),$$

where the dimensionless 'time'  $\tau(z)$ , a function  $B(z)$  describe the evolution of perturbations in the Zel'dovich theory and the parameter  $q_0 \ll 1$  characterizes the coherent length of the initial density field (DD99, DD02, Sec. 7.5).

For low density cosmological models from observations at small redshifts it is possible to deduce that

$$\tau_0 \approx 0.27 \sqrt{\frac{\Omega_m h}{0.2}}, \quad B(z) \approx \left( \frac{1 + 1.2\Omega_m}{2.2\Omega_m} \right)^{1/3} \frac{1}{1+z}, \quad (9)$$

and  $B(z) \approx 1.27/(1+z)$  for  $\Omega_m = 0.3$ . More details are given in DD99 and DD02.

Strictly speaking, relations (6) and (8) are valid for pancakes formed at the same redshift  $z$  and later on the DM column density is changed due to their transverse expansion or compression. However, as was shown in DD02, these processes do not change the statistical characteristics of pancakes observed at redshift  $z$ . This means that statistically we can consider each pancake as created at the observed redshift.

For the cosmological model with matter dominated by DM the observed Doppler parameter is also closely linked with properties of the DM pancakes. Thus, in Paper II the  $b$ -parameter was identified with the infall velocity of matter into pancakes and was expressed through the DM column density as follows:

$$b \approx u_0(z) \sqrt{\xi^2 + 2\xi}, \quad (10)$$

$$u_0(z) \approx 2.3 l_v H_0 \tau^2 \sqrt{1+z} \approx \frac{310 \text{ km/s}}{(1+z)^{3/2}} \sqrt{\frac{0.13}{\Omega_m h^2}}.$$

This assumption is valid also some time after formation of the pancake but later on due to the pancake relaxation, compression and/or expansion in transverse directions the  $b$ -parameter changes.

As is seen from (10), for  $\langle \xi \rangle$  independent from redshift (8), a systematic variation of the mean Doppler parameter with redshift could be expected. The problem was left open in Paper II (due to limited observational data set) but now, with the more representative sample of absorbers, we see surprisingly weak redshift variations of the mean observed Doppler parameter (see discussion in Secs. 4.1). This means that only small fraction of observed absorbers is 'young' and is described by (10), whereas 'older' relaxed absorbers dominate this sample. The simple model of relaxed absorbers

was already considered in Paper II. Here we substantially improve it.

As is well known, for an equilibrium slab of DM the depth of potential well is

$$\Delta \Phi \approx \frac{\pi G \mu^2}{\langle \rho(z) \rangle \delta} \Theta_\Phi, \quad (11)$$

where a random factor  $\Theta_\Phi$  characterizes the nonhomogeneity of matter distribution across the slab. Analysis of numerical simulations (Demiański et al. 2000) indicates that the relaxation of DM component can be approximately described by the polytropic equation of state with the power index  $\gamma \approx 2$ . In the case, we can expect for the factor  $\Theta_\Phi$

$$\Theta_\Phi = 0.5\gamma/(\gamma-1) \approx 1,$$

The actual distribution of DM component across a slab and the value of  $\Theta_\Phi$  depend upon the relaxation process which is essentially accelerated due to the pancake disruption into the system of high density clouds. This means that the factor  $\Theta_\Phi$  randomly vary from absorber to absorber.

The Doppler parameter is defined by the depth of potential well and for the isentropic gas with  $p_{gas} \propto \rho_{gas}^{5/3}$  trapped within the well, we get

$$b^2 \approx \frac{4}{5} \Delta \Phi \approx \frac{4}{5} \frac{\pi G \mu^2}{\langle \rho(z) \rangle \delta} \Theta_\Phi = \delta_0 b_{bg}^2 \frac{q^2}{\delta} (1+z). \quad (12)$$

$$\delta_0 = \frac{3}{10} \left( \frac{H_0 l_v}{b_{bg}} \right)^2 \Omega_m \Theta_\Phi \approx 4 \cdot 10^3 \Theta_\delta,$$

$$\Theta_\delta = \frac{0.3}{\Omega_m} \left( \frac{0.65}{h} \right)^2 \left( \frac{16 \text{ km/s}}{b_{bg}} \right)^2 \Theta_\Phi.$$

### 2.3.2 Characteristics of gaseous component

The observed column density of neutral hydrogen can be written as an integral over a pancake along the line of sight

$$N_{HI} = \int dx \rho_b x_H = 2 \langle x_H \rangle \frac{\langle n_b(z) \rangle l_v q}{1+z} \frac{0.5}{\langle \cos \theta \rangle}. \quad (13)$$

Here  $\langle x_H \rangle$  is the mean fraction of neutral hydrogen and  $\langle \cos \theta \rangle \approx 0.5$  takes into account the random orientation of absorbers and the line of sight. We assume also that both DM and gaseous components are compressed together and, so, the column density of baryons and DM component are proportional to each other.

However, the overdensity of the baryonic component,  $\delta_b = n_b / \langle n_b \rangle$  is not identical to the overdensity of DM component,  $\delta$ . Indeed, the gas temperature and the Doppler parameter are mainly defined by the characteristics of DM component (12) and the bulk heating and cooling of the gas change the density and entropy of the gas trapped within the DM potential well. Under the assumption of ionization equilibrium of the gas (3) this process is described by the equation

$$\frac{1}{n_b} \frac{dn_b}{dt} = n_b \alpha_{rec}(T) [\varepsilon(T) - T_\gamma/T], \quad T = T_{bg} b^2 / b_{bg}^2, \quad (14)$$

where the recombination coefficient  $\alpha_{rec}(T)$  was given in (4),  $T_\gamma \sim (5-10) \cdot 10^4 \text{ K}$  characterizes the energy injected at a photoionization and

$$\varepsilon(T) \approx 2T_4^{1/4} [1 - 0.3 \ln T_4 + 0.13 T_4^{1/3}], \quad T_4 = T/10^4 \text{ K},$$

describes the radiative cooling for the bremsstrahlung emission and the recombination of hydrogen and helium (Black 1981).

The energy injected at the photoionization,  $T_\gamma$ , depends upon the spectrum of local UV background and it varies randomly with time and location. The gas temperature depends upon the process of formation of DM pancake and it varies because of the pancake expansion and compression and due to the pancake disruption into a system of high density clouds. As is seen from (14), these processes lead to a drift of the baryonic density of pancakes and we can write

$$\delta_b = \kappa_b(z)\delta, \quad (15)$$

This drift is important for high density and low temperature pancakes with  $\alpha_{rec}n_b H(z) \geq 1$  and it is small for low density and high temperature pancakes with  $\alpha_{rec}n_b H(z) < 1$  for which the assumption of ionization equilibrium is also invalid. Properties of such pancakes deserve special investigation but their observed population is very small.

Under the assumption of ionization equilibrium of the gas (3) and neglecting a possible contribution of macroscopic motions to the  $b$ -parameter ( $T \propto b^2$ ), the fraction of neutral hydrogen is

$$\langle x_H \rangle = x_0 \kappa_b(z) \delta \beta^{-3/2} (1+z)^3, \quad \beta = b/b_{bg}, \quad (16)$$

and for the column density of neutral hydrogen we get

$$N_H = N_0 q \delta \beta^{-3/2} (1+z)^5, \quad N_0 = 5 \cdot 10^{12} \text{ cm}^{-2} \Theta_H, \quad (17)$$

$$\Theta_H = \frac{0.13}{\Omega_m h^2} \frac{\kappa_b(z)}{\Gamma_{12}} \frac{0.5}{\langle \cos \theta \rangle} \left( \frac{\Omega_b h^2}{0.02} \right)^2 \left( \frac{16 \text{ km/s}}{b_{bg}} \right)^{3/2},$$

where  $\Gamma_{12}$ ,  $b_{bg}$  and  $x_0$  were defined in (2) and (4).

### 2.3.3 Absorbers characteristics

The above relation together with Eq. (12) allows to relate the observed and the main physical characteristics of absorbers like the Lagrangian thickness,  $q$ , the average gas entropy,  $\Sigma = \ln(F_s/F_{bg})$ , and overdensity,  $\delta$ , as follows:

$$q^3 = \frac{N_H}{N_0 \delta_0} \frac{\beta^{7/2}}{(1+z)^6}, \quad \delta = \delta_0 \frac{q^2}{\beta^2} (1+z), \quad (18)$$

$$\exp(\Sigma) = F_s/F_{bg} = \beta^2/\delta_b^{2/3} = \kappa_b^{-2/3} \beta^2/\delta^{2/3}.$$

The function  $\kappa_b(z)$  cannot be estimated from the measured values of  $b$  and  $N_H$  and further on estimating  $F_s$  we will take  $\kappa_b = 1$ .

The precision of these estimates is moderate and the main uncertainties are generated by the unknown and only approximately known parameters  $b_g$ ,  $\Theta_\Phi$ ,  $\kappa_b$  and  $\Gamma_\gamma$ , which vary – randomly as well as systematically – with redshift. As is seen from (17, 18), these variations distort parameters defined in (18) as follows:

$$q^3 \propto \frac{1}{\Theta_H \Theta_\delta}, \quad \delta^3 \propto \frac{\Theta_\delta}{\Theta_H^2}, \quad F_s \propto \kappa_b^{-2/3} \left( \frac{\Theta_H^2}{\Theta_\delta} \right)^{2/9}. \quad (19)$$

The average thickness of pancakes  $\langle q \rangle$  can be compared with expectations (8) what allows to restrict the possible redshift variations of  $\Gamma_\gamma$  and  $\kappa_b$  and to estimate the combined uncertainty introduced by unknown factors. An independent estimate of this uncertainty can be obtained from the analysis of the mean linear number density of absorbers.

The main characteristic of absorber is their Lagrangian thickness,  $\xi \approx q(1+z)^2$ , evolution of which defines the regular variations of the Doppler parameter,  $b$ , and the DM overdensity,  $\delta$ , and, partly, the variations of the entropy,  $F_s$ . However, the parameters  $b$ ,  $\delta$ , &  $F_s$  include also a random component which integrates the evolutionary history of each pancake such as the relaxation processes after the pancake merging. If the pancake relaxation can be actually described by the polytropic equation of state with the effective power index  $\gamma \approx 2$  then we can discriminate the regular and random variations of  $b$ ,  $\delta$ , &  $F_s$  and introduce the *reduced* characteristics of absorbers,  $v$ ,  $\Delta$  &  $S$ :

$$v = \ln[\beta \xi^{(1/\gamma-1)}],$$

$$\Delta = \ln[(1+z)^3 \delta / \xi^{2/\gamma}] = \ln(\delta_0) - v, \quad (20)$$

$$S = \ln[F_s \xi^{2(5/3-\gamma)/\gamma}] = \text{const.} + \frac{2}{3} \frac{3\gamma-1}{\gamma-1} v.$$

These relations indicate that, in fact, our approximate description uses only one random characteristic, namely,  $v$ , and other characteristics of absorbers are expressed through  $\xi$  &  $v$ . In turn, these characteristics are expressed through observed parameters as follows:

$$\xi \approx (1+z) q = \left( \frac{N_H}{N_0 \delta_0} \right)^{1/3} \beta^{7/6},$$

$$v = \frac{\gamma-7}{6(\gamma-1)} \ln \beta - \frac{\gamma-1}{3\gamma} \ln \left( \frac{N_H}{N_0 \delta_0} \right). \quad (21)$$

The influence of other factors, such as the bulk cooling and heating and variations of the spectrum of UV radiation, distort this description. Furthermore, the gas entropy is not changed in the course of transverse expansion and compression of pancakes while the subpopulation of poorer absorbers is probably formed in the course of adiabatic compression. This means that our reduced characteristics are approximate and they must be evaluated directly for the observed sample of absorbers.

More detailed analysis implies the separation of several subpopulations of absorbers with different evolutionary histories that requires more rich sample of observed absorbers.

### 2.4 Mean linear number density of absorbers

Following Paper I we will characterize the mean linear number density of absorbers by the dimensionless function

$$n_{abs} = \frac{c}{H_0} \langle l \rangle^{-1} = \frac{H(z)}{H_0} \frac{dN(z)}{dz}. \quad (22)$$

Here  $dN(z)$  is the mean number of absorbers between  $z$  and  $z+dz$ ,  $\langle l(z) \rangle$  is the mean free path between absorbers at redshift  $z$  and  $c$  is the speed of light. When absorbers are identified with the Zel'dovich pancakes, this mean linear number density can be linked with the fundamental characteristics of the cosmological model and the initial power spectrum.

As was shown in DD02, for the CDM model with heavy DM particles and for richer DM pancakes with thickness significantly larger than the size of density fluctuations, this linear number density can be approximated by

$$n_{abs} \approx \frac{c}{H_0 l_v} \frac{W_p(\xi_{thr})(1+z)^2}{\langle q(\xi_{thr}) \rangle}, \quad (23)$$

$$\langle q(\xi_{thr}) \rangle = 4\tau^2 \left[ 1 + \frac{4\sqrt{\pi\xi_{thr}}\text{erf}(\sqrt{\xi_{thr}}) + 2\exp(-\xi_{thr})}{\pi\exp(\xi_{thr})[1 - \text{erf}^2(\sqrt{\xi_{thr}})]} \right],$$

$$W_p(\xi_{thr}) \approx 0.5[1 - \text{erf}(\sqrt{\xi_{thr}})],$$

where  $\xi_{thr}(z) = q_{thr}/8\tau^2(z)$ ,  $q_{thr}(z)$  and  $\langle q(\xi_{thr}) \rangle$  are the minimal (threshold) and mean Lagrangian thickness of observed absorbers,  $W_p(\xi_{thr})$  is the fraction of matter accumulated by absorbers with  $q \geq q_{thr}$  and a factor  $(1+z)^2$  describes the cosmological expansion of pancake population.

The expression (23) contains only one fitting parameter,  $\xi_{thr}$ , and it successfully describes the evolution of richer absorbers. However, application of this relation to evolution of weaker absorbers is problematic as for  $\xi_{thr} \ll 1$  we get from (23):

$$n_{abs} \approx 90(1+z)^2 B^{-2} \approx 55(1+z)^4,$$

and this relation does not contain any fitting parameters.

Of course, the expression (23) describes only the DM pancakes and formation of the observed gaseous absorbers can be restricted near the Jeans scale what decreases  $W_p(z)$ . The Jeans scale is

$$q_J \approx \frac{b_{bg}(1+z)}{l_v H(z)} \approx 4 \cdot 10^{-3} \sqrt{\frac{4}{1+z} \frac{\Omega_m h^2}{0.13} \frac{b_{bg}}{16 km/s}}, \quad (24)$$

and for  $q \leq q_J$  formation of absorbers is suppressed. For the cosmological model under consideration with  $\langle q \rangle \sim (1+z)^{-2}$  the impact of gaseous pressure becomes essential at  $z \geq 4$ , when  $q_J \sim 0.1\langle q \rangle$ .

For the WDM model, when properties of weaker absorbers and, in particular, their threshold size are restricted by the coherent length of the initial density field, slower redshift evolution of  $n_{abs}$  is expected (DD02):

$$n_{abs} \approx \frac{c}{H_0 l_v} \frac{\sqrt{3}(1+z)^2 \text{erf}(\sqrt{\xi_{thr}})}{16\tau(z)\sqrt{q_0} \sqrt{\xi_{thr}}} \exp(-\xi_{thr}), \quad (25)$$

where again  $\xi_{thr}(z) = q_{thr}(z)/8\tau^2$  and the value  $q_0$  characterizes the coherent length of the initial density field.

For  $q_{thr} = \text{const.}$ , both expressions, (23) and (25), take into account only the processes of pancakes formation and their merging. However, as was shown in DD02 if the observed redshift is identified with the redshift of pancake formation then both relations remain the same even when the transverse compression and/or expansion of pancakes is taken into account.

## 2.5 Observational restrictions

The completeness of observed samples of absorbers is restricted by the condition  $N_H \geq N_{thr} \approx 10^{12} \text{cm}^{-2}$  that in turn distorts the characteristics of observed absorbers and makes it difficult to compare them with the theoretical expectations discussed in Secs. 2.3 and 2.4. This means that these expectations should be corrected for the impact of the threshold column density of observed absorbers.

Thus the investigation of spatial distribution of galaxies in the SDSS EDR (Doroshkevich, Tucker & Allam 2002) results in estimates of typical parameters of galaxy walls at small redshifts as

$$\langle q \rangle \approx 0.4, \quad \langle \beta \rangle \approx 20, \quad \langle \delta \rangle \approx 3. \quad (26)$$

With these data we have for the expected column density of neutral hydrogen within the typical wall (13)

$$N_H \approx 0.02 N_0 \approx 0.1 N_{thr} \Theta_H \leq N_{thr}.$$

This means that even so spectacular objects as the 'Greet Wall' do not manifest themselves as absorbers. Rare absorbers with  $b \geq 100 \text{ km/s}$ ,  $N_H \sim 10^{13} \text{cm}^{-2}$  and  $q \sim 0.1 - 0.2$  observed at  $z \sim 1.5 - 4$  can be associated with embryos of wall-like elements of Large Scale Structure of the Universe (see Sec. 5 for more detailed discussion).

The expected parameters of absorbers associated with 'young' pancakes can be also roughly estimated for  $z \geq 1.5$ . For such pancakes the Doppler parameter is given by (10) and we get for the richer 'young' pancakes with the mean DM column density

$$\xi \approx 1, \quad q \approx \langle q \rangle \approx (1+z)^{-2}, \quad \beta \approx 35(1+z)^{-3/2},$$

$$\delta \approx 3 \Theta_\delta, \quad N_H \approx 10^{-2}(1+z)^{21/4} N_0 \Theta_\delta, \quad (27)$$

and such pancakes can be seen as absorbers already at redshifts  $z \geq 1$ .

For more numerous poorer pancakes with  $q \leq \langle q \rangle \approx (1+z)^{-2}$  we have

$$\beta \sim 30\sqrt{q}(1+z)^{-1/2}, \quad \delta \approx 4q(1+z)^2 \Theta_\delta, \quad (28)$$

$$N_H \approx 2.5 \cdot 10^{-2} N_0 q^{5/4} (1+z)^{31/4} \Theta_\delta$$

$$\approx \left( \frac{q}{0.02} \right)^{5/4} \left( \frac{1+z}{2.5} \right)^{31/4} N_{thr} \Theta_\delta \Theta_H,$$

and such pancakes become visible for  $z \geq 1.5$  only.

These rough estimates of expected characteristics of absorbers show that at redshifts  $z \leq 1.5$  we can observe mainly old pancakes formed at higher redshifts which preserved the measurable column density of neutral hydrogen up to small redshifts. These estimates show also that the expected linear number density of observed absorbers rapidly increases at redshifts  $z \sim 1.5 - 2$  when even relatively poor 'young' pancakes can pass over the observational threshold and can be seen as weak absorbers.

This means that our analysis can be applied to absorbers observed at  $z \geq 1.5 - 2$  when the impact of the observational threshold becomes moderate.

## 2.6 Variations of the UV background

Direct estimates of the intensity of UV background through the proximity effect (see review in Rauch 1998) give results with a moderate precision (factor  $\sim 3 - 5$ ) but cannot be used to test the possible redshift variations of the background. However, indirect estimates of such variations (Songaila 1998) demonstrate the probable sudden drop of the UV intensity of about 4 times at redshifts  $z \sim 3$ . This effect can be related to the strong ionization of HeII at these redshifts (Jacobsen et al. 1994; Zeng, Davidsen & Kriss 1998).

In this paper we discuss similar variations of the UV background seen in the redshift distribution of weaker absorbers at  $z \approx 2.5$  (Sec. 6.2). These variations can be fitted by the expression

$$\Gamma_{12} = \Gamma_0 \frac{a_0 + 1}{2} \left[ 1 + \frac{a_0 - 1}{a_0 + 1} \text{th} \left( \frac{z - z_\gamma}{0.16} \right) \right], \quad (29)$$

where  $\Gamma_0 \sim 1 - 5$  characterizes the intensity of UV background at  $z \ll z_\gamma$ ,  $a_0 \sim 4 - 6$  and  $z_\gamma \sim 2.5 - 3$  characterize

**Table 1.** QSO spectra used

	$z_{em}$	$z_{min}$	$z_{max}$	FWHM km/s	No of HI lines
0000 – 260 <sup>1</sup>	4.11	3.4	4.1	7	431
0055 – 259 <sup>2</sup>	3.66	3.0	3.6	–	534
0014 + 813 <sup>3</sup>	3.41	2.7	3.2	8	262
0956 + 122 <sup>3</sup>	3.30	2.6	3.1	8	256
0302 – 003 <sup>3,2</sup>	3.29	2.6	3.1	8	356
0636 + 680 <sup>3</sup>	3.17	2.5	3.0	8	313
1759 + 754 <sup>4</sup>	3.05	2.4	3.0	–	307
1946 + 766 <sup>5</sup>	3.02	2.4	3.0	8	461
1347 – 246 <sup>2</sup>	2.63	2.1	2.6	–	361
1122 – 441 <sup>2</sup>	2.42	1.9	2.4	–	353
2217 – 282 <sup>2</sup>	2.41	1.9	2.3	–	262
2233 – 606 <sup>6</sup>	2.24	1.5	2.2	–	293
1101 – 264 <sup>2</sup>	2.15	1.6	2.1	–	277
0515 – 441 <sup>2</sup>	1.72	1.5	1.7	–	76
2126 – 158 <sup>7</sup>	3.26	2.9	3.2	11	130
1700 + 642 <sup>8</sup>	2.72	2.1	2.7	15	85
1225 + 317 <sup>9</sup>	2.20	1.7	2.2	18	159
1331 + 170 <sup>10</sup>	2.10	1.7	2.1	18	69

1. Lu et al. (1996), 2. unpublished, courtesy of Dr. Kim 3. Hu et al., (1995), 4. Djorgovski et al. (2000) 5. Kirkman & Tytler (1997), 6. Cristiani & D’Odorico (2000), 7. Giallongo et al. (1993), 8. Rodriguez et al. (1995), 9. Khare et al. (1997), 10. Kulkarni et al. (1996).

the amplitude and the redshift of these variations. These estimates can be distorted due to nonhomogeneous redshift distribution of observed absorbers plotted in Fig. 1.

### 3 THE DATABASE.

The present analysis is based on the 18 spectra listed in Table 1. The available Ly- $\alpha$  lines were arranged into four samples. One of them,  $S_{14}^{12}$ , includes 4454 lines with  $N_H \geq 10^{12} \text{ cm}^{-2}$  from the first 14 high resolution spectra. Two other samples,  $S_{18}^{13}$  and  $S_{18}^{14}$ , include 2740 and 710 lines from all 18 spectra for  $10^{13} \text{ cm}^{-2} \leq N_H$  and  $10^{14} \text{ cm}^{-2} \leq N_H$ , respectively. The sample  $W_{14}^{12}$  contains 2126 weaker lines with  $N_H \leq 10^{13} \text{ cm}^{-2}$  from the first 14 QSOs.

The sample  $S_{18}^{13}$  is the most reliable as these lines are more easily identified and they are not so sensitive to outer random influences. The sample  $S_{14}^{12}$  is partly incomplete but it is the most interesting because it incorporates absorbers in a wide range of  $N_H$ . The samples  $W_{14}^{12}$  and  $S_{18}^{14}$  are used to characterize variations of the UV background and properties of richer absorbers.

The redshift distribution of lines plotted in Fig. 1 is clearly nonhomogeneous and the majority of lines are concentrated at  $z \approx 2$  and  $z \approx 3$ . This means that some of discussed absorber characteristics relate mainly to these ranges of redshift. Absorbers at  $z \geq 3.5$  were identified mainly from the spectrum of QSO 0000-260 (Lu et al. 1996) and here the line statistics is insufficient.

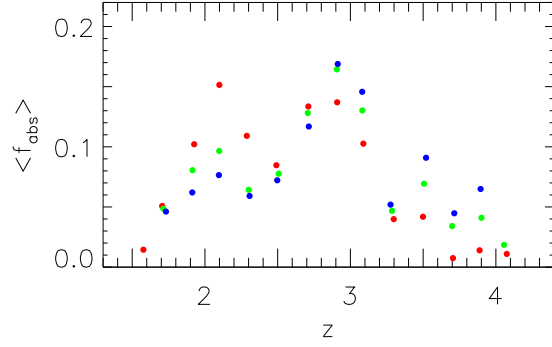


**Figure 1.** Redshift distribution of the observed absorbers for samples  $W_{14}^{12}$  (red points),  $S_{18}^{13}$  (green points) and  $S_{18}^{14}$  (blue points).

### 4 STATISTICAL CHARACTERISTICS OF ABSORBERS

Functions  $q, \delta$  &  $F_s$  discussed in this Section are found for the  $\Lambda$ CDM cosmological model with  $\Omega_m = 0.3, \Omega_\Lambda = 0.7, \Omega_b h^2 = 0.02$ , and for  $\Theta_H = \Theta_\delta = 1$  with redshift variations of the UV background as given by (29) for  $\Gamma_0 = 1, a_0 = 4$ , &  $z_\gamma = 2.5$ . The quantitative results of this Section depend on the uncertain value of the amplitude,  $\Gamma_0$ , and influence of other factors through the relations (19).

For the samples under consideration, only  $\sim 520$  absorbers with  $b \leq b_{bg}$  and  $N_H \leq 10^{13} \text{ cm}^{-2}$  can be related to the artificial “noise”. Their redshift distribution is approximately homogeneous and they cannot influence essentially the measured properties of absorbers. On the other hand, the analysis of the distribution functions (Sec. 4.3) shows some deficit of weaker absorbers what indicates possible small contribution of “noise”.

#### 4.1 Redshift variations of mean characteristics of absorbers

##### 4.1.1 Redshift variations of the observed characteristics

Redshift variations of two observed characteristics of absorbers,  $\langle \beta \rangle = \langle b/b_{bg} \rangle$ , and  $\langle \lg(N_H/N_{min}) \rangle$ , are plotted in Fig. 2 for the samples  $W_{14}^{12}, N_{min} = 10^{11} \text{ cm}^{-2}$ ,  $S_{14}^{12}, N_{min} = 10^{12} \text{ cm}^{-2}$  and  $S_{18}^{13}, N_{min} = 10^{13} \text{ cm}^{-2}$ . Both mean values of  $\langle \beta \rangle$  and  $\langle \lg(N_H/N_{min}) \rangle$  demonstrate surprisingly weak random variations with redshift and for all three samples  $\langle b \rangle \approx \text{const.}$  For the samples  $S_{14}^{12}$  &  $S_{18}^{13}$ ,  $\langle b \rangle = (1.9 \pm 0.17)b_{bg}$  &  $(2.1 \pm 0.16)b_{bg}$  with the scatter  $\sim 8\%$  only. At the same time, the mean Doppler parameter demonstrates systematic shifts from  $\langle b \rangle = (1.6 \pm 0.18)b_{bg}$  for the sample  $W_{14}^{12}$  up to  $\langle b \rangle = (2.4 \pm 0.17)b_{bg}$  for the sample  $S_{18}^{14}$  that indicates weak correlation of observed properties of absorbers. These results are consistent with those obtained in Kim, Cristiani & D’Odorico (2002) and Kim et al. (2002).

The systematic redshift variations of  $\lg N_H$  are roughly fitted by the function

$$N_H \propto (1+z)^{p_h}, \quad (30)$$

with  $p_h = 2$  for the sample  $S_{14}^{12}$  and  $p_h = 1$  for the samples  $W_{14}^{12}$  and  $S_{18}^{13}$ .

The small variations of  $\langle b \rangle$  with the redshift indicate similar small variations of the depth of potential wells,  $\langle \Delta \Phi \rangle$

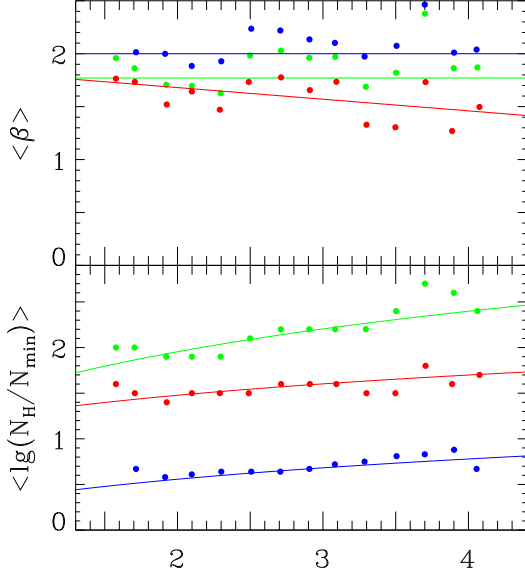


**Figure 2.** Redshift distribution of mean Doppler parameter (top panel) and the mean  $\lg(N_H/N_{min})$  (bottom panel) for samples  $W_{14}^{12}$  (red points),  $S_{18}^{13}$  (blue points), and  $S_{14}^{12}$  (green points). Mean values of  $\langle \beta \rangle$  and fit (30) are plotted by straight lines.

(11), and a correlation between the DM column density,  $q$ , and the overdensity of absorbers,  $\delta$  described by (18). The nature of so weak redshift evolution of  $\langle b \rangle$  remains a mystery.

#### 4.1.2 Redshift variations of DM column density

Other characteristics of absorbers depend upon the physical model used for the interpretation. For the model discussed in Sec. 2 (Eq.18) the redshift variations of the mean DM column density,  $\langle q \rangle$ , the mean entropy and overdensity,  $\langle F_s/F_{bg} \rangle$  and  $\langle \delta \rangle$ , obtained for the redshift variations of the UV background as given by (29) with  $\Gamma_0 = 1$ ,  $a_0 = 4$  and  $z_\gamma = 2.5$  are plotted in Fig. 3.

The DM column density of absorbers,  $q$ , is the most stable parameter which, in principle, is changed due to the successive merging of absorbers and we expect that  $\langle q(z) \rangle$  only weakly depends on the transverse compression and expansion of absorbers (DD02). Action of these factors is approximately described by the function

$$q_{exp}(z) = \langle q \rangle \approx 8\tau^2(z) \approx (1+z)^{-2}.$$

The expression (18) for the DM column density of an individual absorber takes approximately into account the possible variations of the overdensity,  $\delta$ , and Doppler parameter  $\beta$ . Therefore, the differences between the expected,  $q_{exp}$ , and measured,  $\langle q(z) \rangle$ , values characterize, in fact, the influence of factors excluded from the model (18) mainly the intensity of the UV background, redshift variations of ratio  $\delta_b/\delta = \kappa(z)$  (15), and the disruption of pancakes into a system of high density clouds.

All absorbers in considered samples are transparent for the UV background and its redshift variations do not change the shape of HI distribution function,  $N(N_H)$ , and only shifts it along the  $N_H$  axis. However, as was discussed in Sec. 2.5, the sample of observed absorbers and the mean

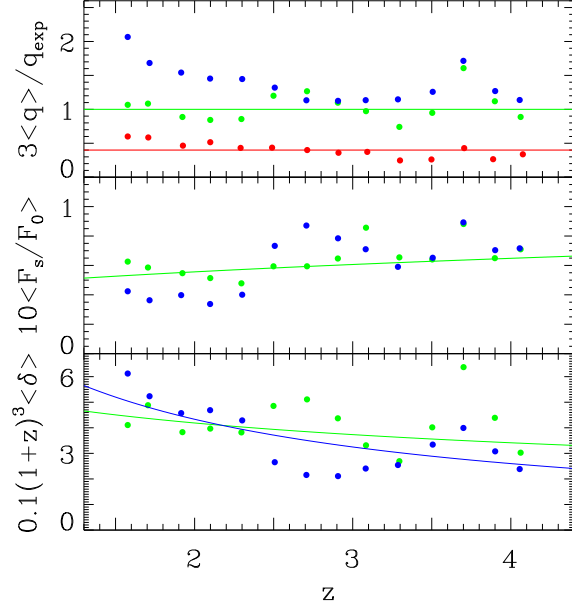


**Figure 3.** Functions  $\langle q \rangle/q_{exp}$  (top panel),  $10(1+z)^{-2}\langle F_s \rangle/F_{bg} = 10\langle F_s \rangle/F_0$  (middle panel) and the overdensity  $0.1(1+z)^3 \langle \delta \rangle$ , (bottom panel) are plotted vs. redshift,  $z$ , for samples  $S_{14}^{12}$  (green points),  $W_{14}^{12}$  (red points) and  $S_{18}^{13}$  (blue points). Rough fits (32) are plotted by lines.

DM column density,  $\langle q(z) \rangle$ , depends also upon the threshold HI column density restricting the sample under investigation what can change the fraction of weaker absorbers and influence the mean measured characteristics of absorbers.

When we assume that the UV background is not changed with redshift then the systematic weak trends

$$\langle q \rangle \approx 0.37[1 + 0.17(1+z)]q_{exp},$$

$$\langle q \rangle \approx 0.17[1 + 0.34(1+z)]q_{exp},$$

appear for the samples  $S_{18}^{13}$  &  $S_{14}^{12}$ , respectively. As is seen from Fig. 3, introduction of the variations (29) eliminates these systematic trends and for the same samples we have

$$\langle q \rangle \approx (0.33 \pm 0.07)q_{exp}, \quad \langle q \rangle \approx (0.21 \pm 0.04)q_{exp}, \quad (31)$$

This result favors redshift variations of the UV background discussed in Secs. 2.6 & 6.3. At small redshifts,  $z \leq 2$ , the influence of the observational restrictions discussed in Sec. 2.4 can suppress the fraction of weaker absorbers and increase the measured value of  $\langle q \rangle$ .

For the sample  $W_{14}^{12}$ , the redshift variations of the measured mean DM column density,  $\langle q \rangle$ , are approximately consistent with theoretical expectations. The small value of this ratio,  $\langle q \rangle \approx 0.1q_{exp}$  could be a result of rejection of absorbers with larger  $N_H$  and  $q$ , an excess of poorer artificial absorbers and underestimates of the parameter  $\Gamma_{12}$ .

Even for the samples  $S_{18}^{13}$  &  $S_{14}^{12}$  we have  $\langle q \rangle \approx (0.2 - 0.3)q_{exp}$  at all redshifts. This fact indicates that the choice  $(\Theta_\delta \Theta_H)^{-1/3} \approx 2-3$  gives a more adequate description of the observed samples. Differences between  $\langle q \rangle$  and  $q_{exp}$  can be enhanced due to a deficit of relatively rare richer absorbers and an excess of artificial poorer absorbers ("noise") in the observed samples and their variations with redshift. However, the action of these factors cannot be strong as the



PDF of the DM column density,  $N_q$ , discussed in Sec. 4.3 is quite consistent with the expected one (8).

The minimal DM column density of absorbers in both samples  $S_{18}^{13}$  and  $S_{14}^{12}$ ,  $\langle q_{thr} \rangle \sim 3 \cdot 10^{-3}$ , only weakly depends upon the redshift. This value is close to the Jeans scale (24) what suggests possible influence of the gaseous pressure on the properties of poorer absorbers. However, this column density is also smaller than the estimate  $q_{thr} \approx (1 - 2) \cdot 10^{-2}$  obtained in Sec. 6.3 (43) from the analysis of redshift distribution of absorbers what again favors the choice  $(\Theta_\delta \Theta_H)^{-1/3} \approx 2 - 3$ .

#### 4.1.3 Redshift variations of overdensity and entropy of absorbers

For all samples plotted in Fig. 3, the redshift dependence of the functions,  $\langle \delta \rangle$ , and  $\langle F_s/F_{bg} \rangle$ , characterizing the overdensity of DM component and entropy of gaseous component can be roughly fitted as follows:

$$(1+z)^3 \langle \delta \rangle \approx \frac{6.5}{\sqrt{1+z}}, \quad (1+z)^3 \langle \delta \rangle \approx \frac{13}{1+z}, \quad (32)$$

$$\langle F_s/F_0 \rangle = (1+z)^{-2} \langle F_s/F_{bg} \rangle \approx 0.4(1+z)^{0.3},$$

where  $F_0$  was defined by (5). These fits emphasize the regular character and general tendencies of absorbers evolution. They show that for the majority of absorbers the bulk cooling exceeds the radiative heating and, therefore  $\langle \kappa_b(z) \rangle \geq 1$ .

These estimates are obtained for  $\Theta_H = \Theta_\delta = 1$  and may be rescaled according to (19). Let us note, however, that both results (31) and  $\langle \delta \rangle \leq 1$  found for  $z \geq 2.5$  verify that this choice is inconsistent with the model under discussion and the choice  $\Theta_H \sim 0.1 - 0.2$  eliminates these disagreements.

#### 4.2 The mean size of absorbers

This model allows also to roughly estimate the real sizes of absorbers along the line of sight,  $\Delta r$ . Due to the strong correlation between  $q$  and  $\delta$ , this size should be obtained by averaging  $\Delta r$  as given by (7). For both samples,  $S_{14}^{12}$  and  $S_{18}^{13}$ , we have

$$\langle \Delta r \rangle \approx 120 - 160 h^{-1} \text{ kpc}, \quad (33)$$

with a scatter  $\sim 10\%$  and this size increases up to  $200 h^{-1}$  kpc for weaker absorbers of the sample  $W_{14}^{12}$ . The observed size of absorbers can also be associated with the Doppler parameter,  $b$ , as

$$\langle \Delta r_b \rangle = 2 \langle b \rangle / H(z) \approx 140 \left( \frac{4}{1+z} \right)^{3/2} h^{-1} \text{ kpc},$$

what is close to the estimate (33). The expected mean transverse size of absorbers is comparable with their Lagrangian size along the line of sight and was roughly estimated in DD02 as

$$\langle \Delta r_t \rangle \approx 5.2 l_v \frac{\tau^2}{1+z} \approx \frac{0.6 l_v}{(1+z)^3} \approx 250 h^{-1} \text{ kpc} \left( \frac{4}{1+z} \right)^3. \quad (34)$$

Difference between the estimated absorber sizes,  $\langle \Delta r \rangle$  and  $\langle \Delta r_t \rangle$ , agrees with expectations of Zel'dovich theory and indicates that such absorbers could be unstable with respect to

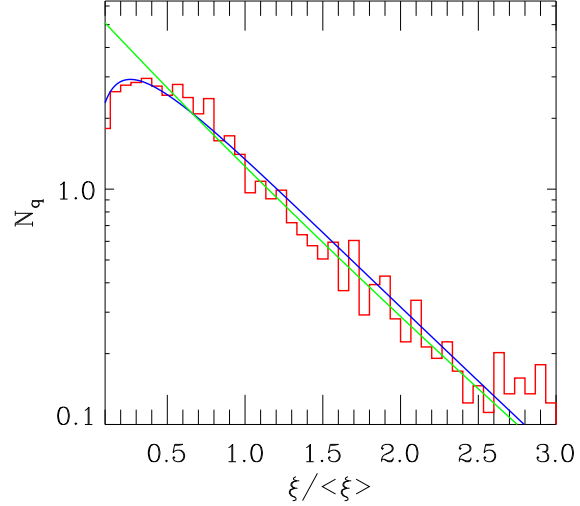


**Figure 4.** PDFs of the Lagrangian pancake thickness,  $N_q$ , for the samples  $S_{14}^{12}$  (red lines). Fits (8) and (35) are plotted by green and blue lines.

the disruption into a system of more compact but less massive clouds with  $\Delta r_t \sim \Delta r$  (see, e.g., Doroshkevich 1980; Vishniac 1983).

#### 4.3 Distribution functions of absorber parameters

The observed PDF of DM size of absorbers can be compared with the expected one (8). However, parameter, overdensity and entropy we can approximately estimate only the influence of the DM size of absorbers whilst the action of wide set of random factors cannot be satisfactory described.

Indeed, the relaxation of DM pancakes depends upon unknown internal structure of pancakes, the adiabatic compression and expansion of an absorber changes its overdensity and temperature. On the contrary, the radiative cooling and bulk heating lead to the drift of the gas entropy and overdensity but retain unchanged the depth of potential well formed by DM distribution. Merging of pancakes increases more strongly the depth of potential well and the gas entropy but the overdensity of the gaseous component increases only moderately. All the time, the temperature and overdensity of trapped gas are rearranged in accordance with the condition of hydrodynamic equilibrium across the pancake.

Because of this, our discussion of absorbers evolution has phenomenological character. The probability distribution functions (PDFs) of the DM pancake sizes,  $\xi$ , is plotted in Fig. 4 for the sample  $S_{14}^{12}$  together with the theoretical fit (8). The distribution functions of the reduced Doppler parameter,  $v$ , and reduced entropy of the gas,  $S$ , for samples  $S_{18}^{13}$  and  $S_{14}^{12}$  are plotted in Fig. 5 together with the Gaussian fits.

##### 4.3.1 Distribution functions of the DM pancake size

The PDF for the Lagrangian size of pancakes,  $N_q(q)$ , plotted in Fig. 4 for samples  $S_{14}^{12}$  is the most interesting because it can be compared with the theoretically expected PDF (8) which, in particular, is sensitive to the coherent length of initial density field,  $q_0$ . As is seen from (8), the PDF  $N_q(\xi)$ ,

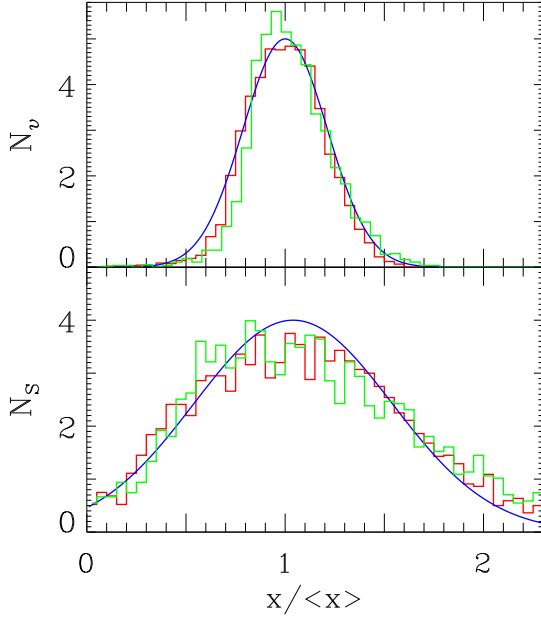


**Figure 5.** PDFs of the reduced Doppler parameter,  $N_v$ , and entropy,  $N_s$ , for the samples  $S_{18}^{13}$  and  $S_{14}^{12}$  (green and red lines, respectively). Gaussian fits are plotted by blue lines.

$\xi \approx q(1+z)^2$ , is weakly dependent on the redshift and, so, we use this PDF for absorbers observed at different redshifts.

For  $\xi \geq 0.5\langle\xi\rangle$ , the PDF plotted in Fig. 4 is well fitted by the function (8) for  $q_0 = 0$  and  $\langle\xi\rangle = 1.22$  instead of the expected value  $\langle\xi\rangle = 0.82$ . This difference is explained by the deficit of absorbers with  $\xi \leq 0.5\langle\xi\rangle$  which can be related to the incompleteness of the observed sample for small  $N_H$  and  $b$ . This result verifies the self-consistency of the physical model used here and the Gaussianity of initial perturbations.

However, as it is seen from (8), this deficit of weaker absorbers can be related also to the suppression of the formation of poorer pancakes caused by the strong correlations of small scale initial perturbations and described by the parameter  $q_0$  in (8). Indeed, the observed PDF is well fitted also by the function

$$N_q = 8 \frac{\text{erf}(\sqrt{y})}{\sqrt{y}} \frac{\exp(-y^2)}{(1 + 0.5/y^2)^{3/4}}, \quad y^2 = 1.3 \frac{\xi}{\langle\xi\rangle}. \quad (35)$$

This fit allows to obtain the rough estimate  $q_0 \approx 0.05$ . This value is very sensitive to the incompleteness of the observed sample at small  $\xi \leq \langle\xi\rangle$  and can be considered only as an upper limit of  $q_0$ .

#### 4.3.2 Distribution functions of the reduced Doppler parameter and entropy

As was noted above, now the theoretical description of the PDFs of the reduced Doppler parameter, overdensity and entropy of the gas is problematic because they depend upon many random factors. Therefore, here we will restrict our analysis to the fits of observed PDFs taking also into account the correlations of the measured  $q$ ,  $b$ ,  $\delta$  &  $F_s$ .

To adjust the reduced characteristics of pancakes introduced in Eq. (20), we will minimize the correlation of  $\xi$  with  $v$ ,  $\Delta$ , &  $S$ . The adjusted reduced characteristics are defined

**Table 2.** Parameters of five subpopulations of absorbers

	$N_{abs}$	$\langle f_s \rangle$	$\langle \beta \rangle$	$r_{bH}$	$\langle \xi \rangle$	$12\langle F_S \rangle / F_0$	$\langle \delta \rangle$
$S_{18}^{13}$							
f	2683	1.00	2.0	0.05	0.24	5.3	1.7
ad	1323	0.49	1.5	0.56	0.18	2.1	1.3
sh	1125	0.42	2.7	0.18	0.26	9.9	0.8
cl	235	0.09	2.0	0.10	0.50	1.4	8.4
$S_{14}^{12}$							
f	4404	1.00	1.9	0.25	0.17	7.0	1.0
ad	1733	0.39	1.3	0.80	0.13	2.1	0.9
sh	2498	0.57	2.3	0.42	0.17	10.8	0.5
cl	173	0.04	2.0	0.21	0.52	1.4	8.5

$f_s$  is the fraction of absorbers in a subsample,  $\delta \leq \delta_{thr}$ ,  $F_s \leq F_{thr}$  for a subsamples "ad";  $\delta \leq \delta_{thr}$ ,  $F_s \geq F_{thr}$  for a subsample "ch";  $\delta \geq \delta_{thr}$ ,  $F_s \geq F_{thr}$  a subsamples "cl". Estimates are obtained for  $\Theta_H = \Theta_\delta = 1$ .

as follows:

$$v = \ln(\beta \xi^{-0.45}), \quad \Delta = \ln[(1+z)^3 \delta \xi^{-1.1}] = \ln \delta_0 - v, \quad (36)$$

$$S = \ln[F_s \xi^{0.15} / F_0] = \text{const.} + 3.67 v,$$

where  $F_0$  was introduced in (5). These expressions correspond to Eq. (20) with the effective power index of compressed DM component  $\gamma = 1.79$  that is very close to  $\gamma = 2$  discussed in Sec. 2.3.3. With such definition, we get the negligible correlations,  $\leq 0.03$ , between  $\xi$  and other reduced characteristics and a strong correlation  $\approx 1$  between  $v$  and  $\Delta$  &  $S$ . The distribution function  $N_v$  plotted in Fig. 5 is well fitted to the Gauss function with  $\sigma_v \approx 0.2\langle v \rangle$  that demonstrates the universal character of the relaxation process and is well consistent with the assumption of approximate equilibrium of majority of observed pancakes. The more broad shape of the PDF  $N_s$  ( $\sigma_s \approx 0.56\langle S \rangle$ ) plotted in Fig. 5 is also consistent with (36).

These results mean that, in fact, the joint action of all random factors together is summarized in the one random function which can be directly expressed through the observed parameters as follows

$$v \approx 0.485 \ln \beta - 0.147 \ln(N_H / N_0 / \delta_0), \quad \gamma = 1.79. \quad (37)$$

More detailed analysis implies the discrimination of subpopulations of absorbers with different evolutionary histories.

#### 4.4 Three subpopulations of absorbers

The overdensity and entropy of gaseous component of absorbers are directly influenced by the evolution of absorbers. Therefore, as a first step for the more detailed investigation of absorbers evolution, we can approximately separate several subpopulations of absorbers with different overdensities and entropies.

Due to continuous distribution of overdensity and entropy for the full samples, the separation of any subpopulations from these samples is quite arbitrary. Thus, we can roughly discriminate only three main subpopulations of absorbers. The first subpopulation of absorbers, let us call it "ad", with  $\delta \leq \delta_{thr}$  and  $F_s \leq F_{thr}$  was formed mainly in the course of adiabatic and weak shock compression. The second subpopulation, called here "sh", contains absorbers

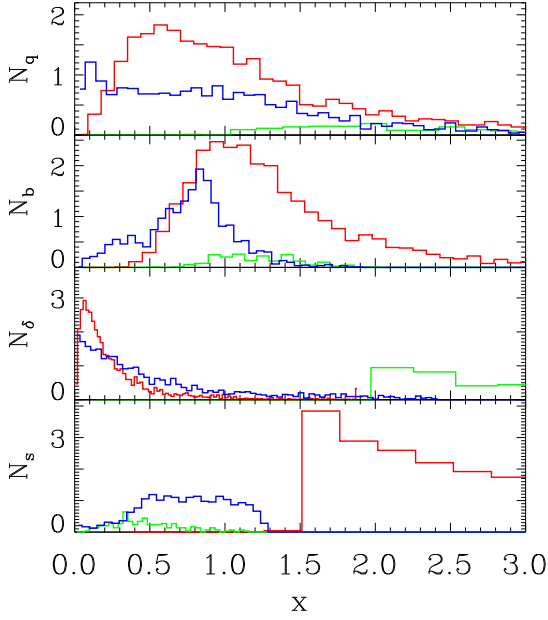


**Figure 6.** For the sample  $S_{14}^{12}$ , the PDFs  $N_q$ ,  $N_b$ ,  $N_\delta$ , and  $N_s$  are plotted for subpopulations "ad" (blue lines), "cl" (green lines) and "sh" (red lines). The arbitrary scales along both axes are used.

with  $F_s \geq F_{thr}$  formed due to shock compression. The third, a rare subpopulation, called here "cl", includes high density and low entropy absorbers with  $\delta \geq \delta_{thr}$  and  $F_s \leq F_{thr}$  for which the radiative cooling is more effective. To select these samples we use two arbitrary threshold values, namely,  $\delta_{thr} = 4$  and  $F_{thr} = 3.6 * [3.5/(1+z)]^2 F_{bg} = 43F_0$  that partly compensates the growth of  $F_{bg} \propto (1+z)^2$ . To avoid high scatter of overdensity, rare objects with  $N_H \geq 10^{16} \text{cm}^{-2}$  were excluded from the consideration.

The mean parameters of these subpopulations are listed in Table 2, where  $r_{bh}$  is the linear correlation coefficient of  $b$  and  $\log N_H$ . From the Table 2 it follows that both samples are dominated by low density and high entropy absorbers with  $\langle \delta \rangle \sim 1$ . This result confirms the inference obtained in Sec. 4.1 that, for the physical model under consideration, the accepted values of  $\Theta_H = 1$  and  $\Theta_\delta = 1$  underestimate both the DM column density,  $q$ , and overdensity of absorbers,  $\delta$ .

In spite of the quite arbitrary choice of threshold parameters this discrimination illustrates correctly the action of evolutionary factors mentioned above, for example, the progressive growth of the fraction of high density cooled pancakes at smaller redshifts. The objective character of the sample discrimination is seen from the comparison of  $\langle b \rangle$  and the linear correlation coefficient,  $r_{bh}$ , of the observed parameters,  $b$  and  $\lg N_H$ , listed in Table 2 for the full samples and for the separated subpopulations.

The Fig. 6 demonstrates correlations between the Doppler parameter, entropy and overdensity of absorbers rooted in definitions (18). Thus, for all subpopulations there is the strong correlation between the Doppler parameter, entropy and the Lagrangian thickness of absorbers,  $r_{bs} \sim 0.5 - 0.7$  and  $r_{bq} \geq 0.7$  while the Doppler parameter and overdensity are significantly correlated only for the "ad" subpopulations.

The redshift distribution of the matter fraction assigned to subpopulations of absorbers plotted in Fig. 7 for the same

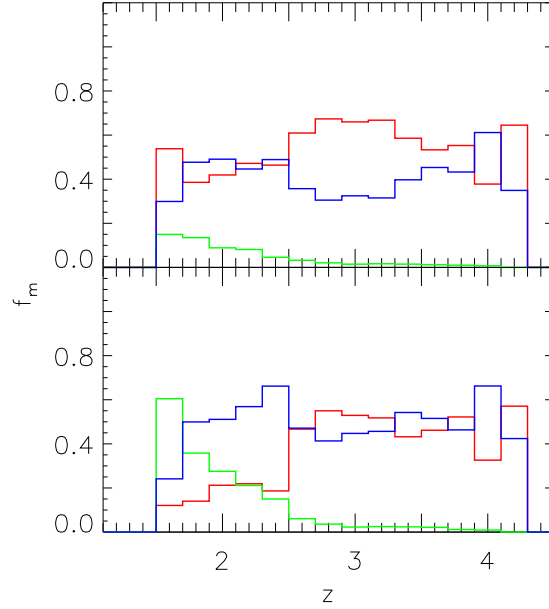


**Figure 7.** The matter fractions assigned to "ad" (blue lines), "cl" (green lines) and "sh" (red lines) subpopulations of absorbers are plotted vs. redshift,  $z$ , for samples  $S_{14}^{12}$  (top panel) and  $S_{18}^{13}$  (bottom panel).

samples demonstrate the growth of concentration of cold absorbers at small redshifts what illustrates the influence of the radiative cooling of gas. The weak variations of subpopulations "ad" and "sh" can be partly caused by the rough method of separation used here which mixes into the "ad" subpopulation also some fraction of rich pancakes formed at higher redshifts and later cooled. Indeed, the redshift evolution of the DM column density discussed in Sec. 4.1.2 indicates the growth of the pancake richness,  $\langle q \rangle$ , for smaller redshifts and, because the adiabatic compression is naturally related to weaker pancakes, we can expect the domination of the "sh" population at small redshifts. As seen in Fig. 6, this inference indicates also that in the "ad" and "sh" subpopulations there are pancakes with the same  $q$ .

Analysis of subpopulations of pancakes with a restricted DM sizes,  $q$ , or with a restricted Doppler parameter,  $b$ , that is with the same depth of potential well, demonstrates strong variations with redshifts of both overdensity and entropy what confirms the complex character of absorbers evolution.

These results illustrate the main evolutionary tendencies in a wide range of redshifts. They indicate that majority of observed absorbers represent pancakes formed in the course of adiabatic and shock compression both near the observed redshifts and earlier. Only  $\sim 10\%$  of the observed absorbers are effectively cooled and their entropy decreased. Only small fraction of absorbers retains high entropy after compression up to high overdensity.

More detailed statistical investigation of absorbers evolution requires finer discrimination of the sample and therefore richer set of observed absorbers is needed.

## 5 WALLS AT HIGH REDSHIFTS

Majority of the rare absorbers with higher Doppler parameter,  $b \geq (80 - 90)\text{km/s}$  and moderate column density of neutral hydrogen  $N_H \leq 10^{15}\text{cm}^{-2}$ , can be identified with the embryos of richer structure elements which are seen now as rich walls in the observed galaxy distribution. As a rule, for such absorbers  $q \sim q_{exp} \approx (1+z)^{-2}$ ,  $\delta \sim 1$  and  $F_s \geq 10F_{bg}$  what verifies this identification.

The number of such absorbers is small and their statistical characteristics cannot be reliably determined. However, as an independent test, we can use the mean comoving separation of such absorbers,

$$D_{sep} = cH_0^{-1}\Omega_m^{-1/2} \Delta z / (1+z)^{3/2}. \quad (38)$$

For 38 separations of absorbers with  $b \geq 90\text{km/s}$  at  $1.8 \leq z \leq 3.8$  selected in 9 spectra we get

$$\langle D_{sep} \rangle \approx (60 \pm 20)h^{-1}\sqrt{0.3/\Omega_m}\text{Mpc}.$$

Such large separation suggests that these objects will retain their individuality up to small redshifts and, indeed, these separations are quite consistent with the mean wall separation  $D_w \approx (66 \pm 13)h^{-1}\text{Mpc}$  measured for the SDSS EDR at  $z = 0$  (Doroshkevich, Tucker & Allam 2002).

The same  $D_{sep}$  is observed for 17 absorbers with  $b \geq 100\text{km/s}$ . However, for smaller  $b$ , the number of absorbers rapidly increases and already for 139 absorbers with  $b \geq 70\text{km/s}$  in 15 spectra the mean separation decreases to  $D_{sep} \sim (40 \pm 20)h^{-1}\text{Mpc}$ .

These results show that the walls begin to form already at  $z \sim 3$  and continue to form up to the present time. At the same time, the continuous distribution of all parameters of absorbers shows that at high redshifts the discrimination of walls and other structure elements is quite arbitrary. The problem deserves further investigation in a wider range of redshifts with a more representative sample of absorption lines especially at high redshifts. Perhaps, such walls can be also observed in the galaxy distribution at high redshifts.

## 6 REDSHIFT DISTRIBUTION OF ABSORBERS

The investigation of the redshift variations of the mean linear number density of absorbers allows to test the adopted physical model of absorbers and to check some characteristics of absorbers discussed above. For weaker absorbers from the sample  $W_{14}^{12}$ , the comparison of measured and expected redshift distributions of  $n_{abs}$  allows to reveal the variations of intensity of UV background.

To obtain independent estimates of the properties of DM component and to minimize the influence of UV background, we have to select samples of absorbers with the same threshold DM column density,  $q_{thr}$ , rather than with the same minimal  $lgN_H$ . Three such samples, namely,  $Q_{18}^{10}$ ,  $Q_{18}^{05}$ , and  $Q_{18}^{01}$  with the threshold  $q_{thr} = 0.01, 0.005$  &  $0.001$  were selected from the full set of absorbers. These samples contain 3080, 4149 and 4811 absorbers, respectively.

The sample  $Q_{18}^{01}$  includes  $\sim 90\%$  of all lines and probably is incomplete because some fraction of weak lines is excluded by the observational limit  $lgN_H \geq 12$ . It can be used for comparison with results obtained for samples  $Q_{18}^{10}$

and  $Q_{18}^{05}$  for which independent estimates of  $q_{thr}$  can be obtained. Such analysis allows to estimate roughly unknown parameters  $\Theta_H$  &  $\Theta_\delta$ . For these samples we can also estimate the parameter  $q_0$  (25) which characterizes the coherent length of initial density field.

Here we also use the sample of HST data (Bahcall et al. 1993, 1996; Jannuzi et al. 1998) which contains 1000 absorbers at  $z \leq 1.5$ . This sample is probably incomplete at least at  $z \geq 1.3 - 1.5$ .

For 8 spectra from Table 1 the redshift distribution of absorbers is discussed also in Kim et al. (2002).

### 6.1 Selection of Poissonian subsamples of absorbers

The first problem is the selection of a Poissonian subsample of absorbers and estimation of their mean linear number density at various redshifts. For this purpose, we use the measured redshift separations of neighboring absorbers,  $\Delta z$ , what partly attenuates the influence of selection effects inherent in individual spectra. This separation is transformed to the dimensionless comoving distance,

$$\Delta l = H_0 \Delta z / H(z),$$

and absorption lines in the interval  $z - dz < z < z + dz$  taken from all spectra under investigation are organized into an 'equivalent single field' by arranging the line separations  $\Delta l$  one after the other along the line of sight. For richer samples, distribution of absorbers obtained in this way is similar to the Poissonian one and the mean linear number density,  $\langle n \rangle$ , can be found using the differential or cumulative distribution functions of separation, namely,

$$dN/dx = \exp(-\langle n \rangle x) / \langle n \rangle, \quad (39)$$

$$N = \exp(-\langle n \rangle x). \quad (40)$$

To decrease uncertainties and to estimate actual scatter of these fits we rejected all points before the maxima of differential PDF and only more representative middle part of PDFs with the fraction of points  $f \leq f_{thr}$  were used. The threshold fraction,  $f_{thr}$ , was varied between  $f_{thr} = 0.7$  and  $f_{thr} = 0.95$ . Mean values and dispersions of the sets of measurement with different  $f_{thr}$  were taken as the actual value and scatter of  $n_{abs}$ . As a rule, the fit (40) of cumulative PDFs gives more stable estimates and smaller error bars than the fit (39) of differential PDFs. Both estimates of  $n_{abs}$  are plotted in Figs. 8 & 9.

### 6.2 Variations of intensity of UV background

For the sample  $W_{14}^{12}$  the redshift distribution of absorbers is plotted in Fig. 8 together with the fit (25) which characterizes roughly the expected redshift distribution of absorbers. The linear number density of weak absorbers in this sample is especially sensitive to variations of intensity of UV background radiation what is clearly manifested in the strong variations of  $n_{abs}$  in comparison to the smooth fitting curve. At  $z \leq 2$  the rapid decrease of  $n_{abs}$  is caused by the influence of the threshold observed column density of neutral hydrogen,  $N_H \geq N_{thr} \approx 10^{12}\text{cm}^{-2}$ , discussed in Sec. 2.5.

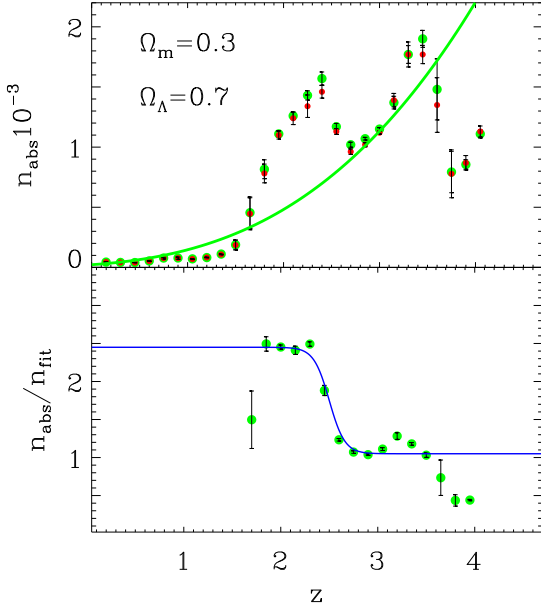


**Figure 8.** Top panel: redshift distribution of  $n_{abs}$  found with fits (39) and (40) (red and green points) for the sample  $W_{14}^{12}$ . Fit (25) is plotted by green line. Bottom panel: redshift variations of  $n_{abs}/n_{fit}$  for the same sample. Fit (41) is plotted by blue line.

The observed variations of  $\langle n_{abs} \rangle$  are roughly fitted to the function

$$\langle n_{abs} \rangle / n_{fit} = 1.75 + 0.7 \operatorname{th} \left( \frac{2.5 - z}{0.16} \right), \quad (41)$$

also plotted in Fig. 8. The same variations but with less amplitude are also seen for absorbers in the sample  $S_{18}^{13}$ .

The column density of neutral hydrogen is proportional to  $\Gamma_{\gamma}^{-1}$  and increase of  $\Gamma_{\gamma}$  shifts weak absorbers under the observational threshold. This means that the relation (41) describes quite well the redshift dependence of variations of UV background but their amplitude depends upon the distribution function of  $N_H$ . Direct estimates show that the variations of the intensity of about 4 – 6 times described by (29) provides the observed variation of  $\langle n_{abs} \rangle$ . As was discussed in Sec. 4.1.1 the same variations of the UV background eliminate also the unexpected variations of the mean DM surface density of absorbers,  $\langle q \rangle$ , what verifies this interpretation. Similar variations of the UV background at  $z = 3$  were discussed in Songaila (1998) and in Theuns, Zaroubi & Kim (2002).

### 6.3 Redshift distribution of DM pancakes

To investigate the redshift distribution of the mean linear number density of DM pancakes we can use the samples  $Q_{18}^{10}$ ,  $Q_{18}^{05}$ , and  $Q_{18}^{01}$  prepared with  $q_{thr}(z) \approx \text{const.}$  Using the relation (25) to fit these distributions we obtain independent estimates of both  $q_{thr}$  and  $q_0$  what allows to test the self consistency of the physical model, to estimate the unknown random parameters as given by (19) and to restrict the shape of initial power spectrum of perturbations.

The redshift distribution of absorbers in the sample  $Q_{18}^{05}$  is plotted in Fig. 9 together with the best fit (25) and the random scatter of observed points around the fit. At redshifts  $z \leq 3.3$  at which the representativity of samples is

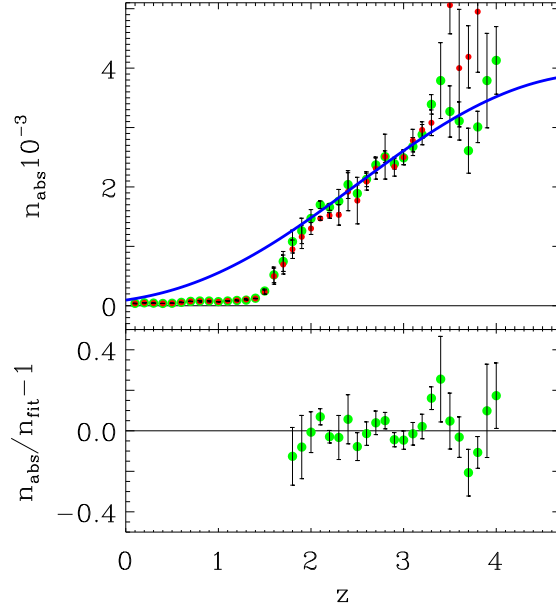


**Figure 9.** Top panel: redshift distribution of  $n_{abs}$  found with fits (39) and (40) (red and green points) for the sample  $Q_{18}^{05}$ . Fit (25) is plotted by the blue line. Bottom panel: Differences between measured and fitted absorber distributions,  $n_{abs}/n_{fit} - 1$ .

better the scatter does not exceed  $\sim 20\%$  what indicates the moderate impact of variations of the UV background.

At redshifts  $z \sim 1.5 - 2$  the rapid growth of observed mean linear number density of absorbers

$$\langle n_{abs} \rangle \propto \left( \frac{1+z}{2.7} \right)^8 \quad (42)$$

coincides with the expected one (28) and it is naturally explained by the influence of observational threshold  $N_H \geq N_{thr} \approx 10^{12} \text{ cm}^{-2}$ . Such cutoff is not seen for the subpopulation of richer absorbers with  $N_N \geq 10^{14} \text{ cm}^{-3}$  what verifies its connection with the observational threshold. The probable incompleteness of the sample of weak absorbers at  $z \leq 1.5$  enhances this rapid growth of  $\langle n_{abs} \rangle$ .

The best estimates of the fit parameters (25) for the samples  $Q_{18}^{10}$ ,  $Q_{18}^{05}$ , and  $Q_{18}^{01}$  are, respectively,

$$q_{thr} \approx (2.3 \pm 0.3) \times 10^{-2}, \quad q_{thr} \approx (2.2 \pm 0.3) \times 10^{-2}, \quad (43)$$

$$q_{thr} \approx (2.1 \pm 0.3) \times 10^{-2},$$

where the formal errors of the fits are given. Comparison of these values of  $q_{thr}$  with those used for the sample selection demonstrates the influence of the noise of weak lines concentrated mainly at larger redshifts and allows to estimate the random factors  $(\Theta_H \Theta_\delta)^{-1/3} \approx 2 - 3$  what is quite consistent with results obtained in Sec. 4.1.2.

For  $q_0$  we have from all three samples

$$q_0 \approx (1.7 \pm 0.3) \times 10^{-2}. \quad (44)$$

These results confirm that the expression (25) fits well the observed redshift distribution of absorbers. However, both estimates (43) and (44) are preliminary and model dependent. They are sensitive to the redshift distribution of the dominant population of weaker absorbers and to quite uncertain variations of the UV background.

The model under discussion can be tested with the red-

shift variations of the mean linear number density of richer absorbers with larger  $q_{thr}$  which is not so sensitive to the UV background. For example, for the sample  $Q_{18}^{10}$  the redshift distribution of absorbers can be also fitted by expression (23) with the same  $q_{thr}$  which is insensitive to the small scale part of the power spectrum. However, the difference between fits (23 & 25) is small at redshifts  $z \leq 3.5$  and becomes essential at larger redshifts where the available statistic of observed absorbers is poor.

These comments show that the estimates (44) of the important parameter  $q_0$  must be considered as the upper limit rather than the actual value.

As was found in Sec. 6.2, the action of the UV background is minimal at redshifts  $1.9 \leq z \leq 2.5$  where the linear number density of observed absorbers is maximal. Therefore, we can use this range of redshifts to improve the estimates (44). But in this case we cannot fit sufficiently accurately the redshift absorber distribution at higher redshifts.

For the sample  $S_{14}^{12}$  at  $1.9 \leq z \leq 2.5$  the best fit parameters are

$$q_{thr} \approx (2.2 \pm 0.8) \times 10^{-2}, \quad q_0 \approx (0.8 \pm 0.2) \times 10^{-2}, \quad (45)$$

where again the formal errors of the fits are given. This value of  $q_{thr}$  is close to that found in (43) what confirms that in this sample contains the same absorbers. However, the growth of the linear number density of absorbers at these redshifts decreases the new estimate of the parameter  $q_0$ .

The sample dependence of our results indicates that the actual reliability and precision of our estimates is limited due to limited representativity of the samples and the unknown random influence of the UV background. This means that even the estimate (45) must be considered as the upper limit rather than as the actual estimate of  $q_0$ . Non the less, these results suggest that the values of  $q_0$  and  $q_{thr}$  should be similar and we can expect that  $q_0 \approx 10^{-2} \geq 10^{-3}$ . This inference is also supported by the shape of the PDF  $N_q$  plotted in Fig. 4. It indicates that the incompleteness of the observed sample of absorbers is moderate.

The model as a whole and estimates of  $q_0$  can be improved with richer sample of absorbers at high redshifts  $z \geq 3.5$ , where the linear number density of absorbers with larger  $q_{thr}$  rapidly decreases. However, as was found in Songaila (1998), at  $z \geq 3$  the random variations of the UV background increase what increases the scatter of  $\langle n_{abs} \rangle$  for weaker absorbers.

#### 6.4 Redshift distribution of absorber separation

As is well known, at redshifts  $z \geq 4$  the absorbers begin to overlap and their separation becomes problematic. Analysis of the evolution of the mean absorber separation allows to quantitatively estimate this effect. For this purpose, we can compare the mean separation of absorbers at various redshifts,  $\langle D \rangle$ , with the mean Doppler parameter which characterizes the observed thickness of absorbers. These values for samples  $S_{14}^{12}$  and  $S_{18}^{13}$  are roughly fitted by power laws:

$$\langle D \rangle \approx \left( \frac{4}{1+z} \right)^{2.6} h^{-1} \text{Mpc}, \quad \frac{H_0 \langle D \rangle}{\langle b \rangle} \approx \left( \frac{6.1}{1+z} \right)^{2.6}, \quad (46)$$

$$\langle D \rangle \approx \left( \frac{4.9}{1+z} \right)^3 h^{-1} \text{Mpc}, \quad \frac{H_0 \langle D \rangle}{\langle b \rangle} \approx \left( \frac{7}{1+z} \right)^3. \quad (47)$$

These results verify that at  $z \sim 5 - 6$  absorbers effectively overlap and the system of individual absorbers is transformed into continuous absorption imitating the Gunn – Peterson effect.

## 7 SUMMARY AND DISCUSSION.

In this paper we continue the analysis initiated in Paper I and Paper II based on the statistical description of Zel'dovich pancakes (DD99, DD02). This approach allows to connect the observed characteristics of absorbers with fundamental properties of initial perturbations and to reveal the main tendencies of structure evolution. It demonstrates also the generic similarity of absorbers and the Large Scale Structure observed in the spatial galaxy distribution at small redshifts.

In this paper we investigate the new more representative sample of  $\sim 5000$  observed absorbers what allows us to improve the physical model of absorbers introduced in Paper I and Paper II and to obtain more detailed description of physical characteristics of absorbers. The progress achieved demonstrates again the key role of the representativity of observed samples for the construction of the physical model of absorbers and reveals a close connection of the possible conclusions with the database used.

However, even richness and representativity of this sample is not sufficient for the more detailed study of some important problems of the structure evolution. Further progress in such investigations requires richer and more representative sample of observed absorbers.

### 7.1 Main results

The main results of our analysis can be summarized as follows:

(i) The approach used in this paper allows to link the observed and other physical characteristics of Ly- $\alpha$  absorbers such as the overdensity and entropy of the gaseous component and the column density of DM component accumulated by absorbers.

(ii) The basic observed properties of absorbers are quite successfully described by the statistical model of DM confined structure elements (Zel'dovich pancakes). Comparison of independent estimates of the DM characteristics of pancakes confirms the self consistency of the adopted physical model.

(iii) The same comparison allows to estimate the unknown parameters of the model (19), for example  $(\Theta_H \Theta_\delta)^{-1/3} \approx 2 - 3$ . This normalization leads to the probable intensity of the UV background  $J(\nu_H) \sim 3 - 6 \cdot 10^{-21} \text{ erg cm}^{-2} \text{ s}^{-1} \text{ sr}^{-1} \text{ Hz}^{-1}$ .

(iv) We show that in the framework of approach used all characteristics of absorbers can be expressed through two functions,  $\xi$  &  $v$ , characterizing the systematic and random variations of absorber properties and directly expressed through the observed parameters,  $N_H$  &  $b$ .

(v) The approach used allows to separate approximately three subpopulations of absorbers with high and low entropy and high and low overdensity, which represent the main stages of the structure evolution.



(vi) The absorbers with high Doppler parameter,  $b \geq 90$  km/s can be naturally identified with the embryos of wall – like structure elements observed in spatial distribution of galaxies at small redshifts.

(vii) Analysis of the redshift distribution of absorbers allows to reveal the probable systematic redshift variations of the UV background.

(viii) The strong suppression of the mean linear number density of absorbers at  $z \leq 1.8$  can be naturally explained by the influence of the observational threshold  $N_H \geq N_{thr} \approx 10^{12} \text{ cm}^{-2}$ .

(ix) We can also estimate the moment  $m_0$  of initial power spectrum, which in turn can be linked with the cutoff of the power spectrum and the mass of dominant fraction of DM component.

These results demonstrate the close link of absorbers and Zel'dovich pancakes and verify that both the properties of absorbers and of the Large Scale Structure in the observed spatial galaxy distribution are closely connected with the initial power spectrum of perturbations. These results demonstrate also the complex composition of observed samples of absorbers what is the main source of difficulties with the description and interpretation of their properties. In particular, we were not able to explain the surprisingly weak redshift variations of the observed Doppler parameter.

## 7.2 Variations of intensity of the UV background

The analysis of redshift variations of the mean linear number density of weak absorbers (Sec. 6.2) reveals the redshift variations of the UV background which can be related to the reionization of HeII (Songaila 1998; Theuns, Zaroubi & Kim 2002) and possible variations of activity of quasars, galaxies and other sources of UV radiation. These variations of the intensity of UV background (29) allow to reduce the difference in redshift variations of expected and measured mean DM column density of absorbers (Sec. 4.1.1).

## 7.3 Absorber properties

The physical model of absorbers introduced in Sec.2 links the measured  $z$ ,  $b$  and  $\lg N_H$  with other physical characteristics of both gaseous and DM components forming the observed absorbers. Some characteristics of DM component can also be found independently from the redshift distribution of absorbers that allows to test the self consistency of our model of absorbers and to estimate the unknown numerical factors of the model.

Analysis of measured  $b$  and  $\lg N_H$  performed in Sec.4 shows that the sample of observed absorbers is composed of pancakes with various evolutionary history. We discuss five main factors that determine the evolution of structure. They are: the transverse expansion and compression of pancakes, their merging, the radiative cooling of compressed gas, and the disruption of structure elements into a system of high density clouds. First two factors change the overdensity of DM and gas but do not change the gas entropy. Next two factors change both the gas entropy and overdensity but do not change the DM characteristics.

With the introduction of *reduced* Doppler parameter,

$v$ , overdensity,  $\Delta$ , and entropy,  $S$ , we can discriminate between the systematic and random variations of properties of observed absorbers. The former can be naturally related to the progressive growth of the DM column density of absorbers described by the function  $\xi(z)$ . In turn, the later caused by the action of discussed random factors cannot be satisfactory describe by any theoretical model. However, our analysis in Sec. 4.3 shows that, in the framework of approach used, the random variations of all three reduced parameters are strongly correlated. In fact, the joint action of all random factors together is summarized in the random function  $v$  which can be directly expressed through the observed parameters (37).

With the entropy and overdensity we can roughly discriminate three subpopulations of absorbers illustrating the influence of factors mentioned above. As is seen from Table 2 and Fig. 6, there is a clear correlation in the distribution of overdensity and entropy of absorbers and, for example, for subpopulation of high entropy absorbers the overdensity is less than for the subpopulation of cold low entropy absorbers. The redshift variations of overdensity and entropy, plotted in Fig. 3 and of the fractions of absorbers assigned to the three subpopulations plotted in Fig.7 demonstrate the progressive cooling of pancakes with time.

Estimates of the size of absorbers (Sec. 4.2) suggest the possible fast disruption of absorbers into a system of high density clouds what is the first step of formation of dwarf galaxies. The limited representativity of the observed sample does not allow to reveal clear traces of this process.

## 7.4 Absorbers as elements of the Large Scale Structure of the Universe

The analysis of the evolution of the mean linear number density of absorbers is very important for the reconstruction of the evolutionary history of the Universe. Thus, the comparison of statistical characteristics of absorbers with those expected for the LSS evolution in models with the Harrison - Zel'dovich initial power spectrum and the spatially flat  $\Lambda$ CDM cosmology shows that some populations of absorbers can be identified with the wall-like elements of the LSS observed in the rich galaxy redshift surveys such as the SDSS EDR.

Indeed, as was shown in Sec. 5, characteristics of the rare absorbers with larger Doppler parameter,  $b \geq 90$  km/s are quite similar to those expected for the embryos of galaxy walls. On the other hand, the connection of absorbers with galaxy filaments is recently confirmed by direct observations by Penton, Stocke & Shull (2002).

For the population of weaker absorbers, the PDF of the DM column density discussed in Sec. 4.3 coincides quite well with the expected one for the Gaussian initial perturbations what verifies their strong link to the Zel'dovich pancakes. As shown in Sec. 6.3 the theoretical relations, (23) and (25), obtained in the framework of the same theory fit reasonably well the observed absorbers distribution. Relation (25) allows to estimate independently the threshold column density of DM component and the shape of initial power spectrum. The fast drop of  $n_{abs}$  at  $z \leq 1.8$  can be naturally related to the influence of the observational threshold  $N_H \geq 10^{12} \text{ cm}^{-2}$ .

This analysis allows to obtain the independent esti-

mates of DM characteristics of pancakes and to test the physical model used in Sec. 4 for the interpretation of measured  $b$  and  $lgN_H$ . Estimates (45) of the  $q_{thr}$  confirm the self consistency of our approach (for  $(\Theta_H \Theta_\delta)^{-1/3}$  2 – 3) and show that for the redshifts under consideration the Jeans scale (24) does not yet suppress formation of observed absorbers. These results indicate that the probable intensity of the UV background is  $\sim (3 - 6) 10^{-21} \text{ erg cm}^{-2} \text{ s}^{-1} \text{ sr}^{-1} \text{ Hz}^{-1}$  what exceeds the available estimates of Cook, Espey & Carswell (1997) by about an order of magnitude.

Finally, our analysis allows to estimate the important parameter  $q_0$  which characterizes the shape of initial power spectrum and properties of the dominant DM component.

### 7.5 Characteristics of the initial power spectrum

The shape and amplitude of large scale initial power spectrum are well established by investigations of relic radiation and the structure of the Universe at  $z \ll 1$  detected in large redshift surveys such as the LCRS (Schechter et al. 1996), SDSS (Stoughton et al. 2001) and 2dF (Efstathiou et al. 2001). However, the shape of small scale initial power spectrum can be tested only at high redshifts where its influence is stronger and it is not yet distorted by nonlinear evolution.

Present discussions on the mass of dominant fraction of DM component and the shape of small scale initial power spectrum are focused on the formation of low mass halos in standard CDM simulations in comparison with observed low mass satellites (see, e.g., Colin, Avila-Reese & Valenzuela 2001; Bode, Ostriker & Turok 2001), and at the simulations of absorbers. Thus, Narayanan et al. (2000) estimate the low limit of this mass as  $M_{DM} \geq 0.75 \text{ keV}$ , while Barkana, Haiman & Ostriker (2001) increase this limit up to  $M_{DM} \geq 1 - 1.25 \text{ keV}$ .

Here we can compare these estimates with the direct measurement of redshift distribution of absorbers. In fact, our estimates are related to two spectral moments of the initial power spectrum,  $m_{-2}$  and  $m_0$ . The first of them depends mainly upon the large scale part of the power spectrum and was estimated from the measured characteristics of observed structure at small redshifts,  $z \ll 1$ . Together with cosmological parameters,  $\Omega_m$  and  $h$ , this moment defines the coherent length of initial velocity field,  $l_v$ , (6), used in Sec. 2.3 for discussion of properties of DM distribution.

The second moment,  $m_0$ , depends upon the small scale part of the power spectrum and upon the shape of transfer function. This means that the estimates of the mass of DM particles are model dependent even though our estimates of  $q_0$  and spectral moments are based on the analysis of observations.

As was shown in DD99 and DD02, for the CDM and WDM models with the Harrison – Zel'dovich asymptotic of power spectrum,  $p(k) \propto k$ , and transfer functions,  $T(k)$ , given in Bardeen et al. (1986) the coherent length of initial density perturbations,  $l_\rho$ , and the parameter  $q_0$  can be written as follows:

$$q_0 = 5 \frac{m_{-2}^2}{m_0}, \quad l_\rho = q_0 l_v \approx 0.34 h^{-1} \text{ Mpc} \left( \frac{q_0}{0.01} \frac{0.2}{\Omega_m h} \right), \quad (48)$$

$$m_{-2} = \int_0^\infty dx x T^2(x) \approx 0.023, \quad m_0 = \int_0^\infty dx x^3 T^2(x),$$

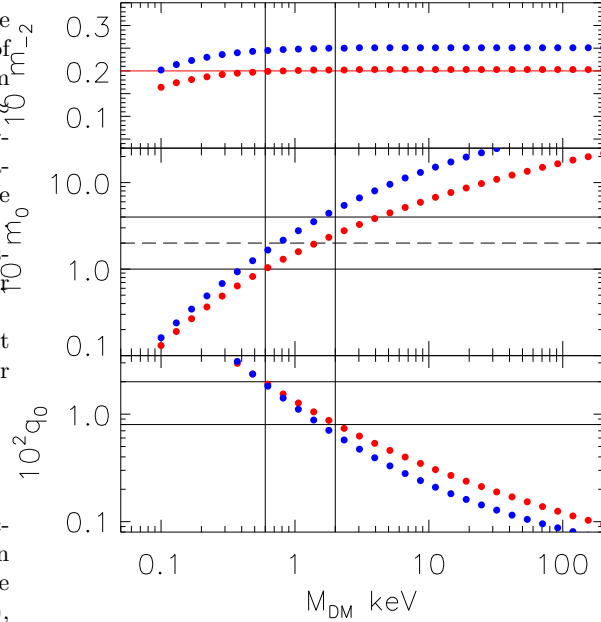


**Figure 10.** Spectral moments,  $m_{-2}$  and  $m_0$ , and the parameter  $q_0$  are plotted for the CDM (red points) and WDM (blue points) power spectra (50). Black lines show the observational restrictions.

$$x = \frac{k}{k_0}, \quad k_0 = \Omega_m h^2 \text{ Mpc}^{-1}, \quad l_v = \frac{1}{k_0 \sqrt{m_{-2}}},$$

where  $k$  is the comoving wave number.

The damping length for WDM particles is

$$R_{fw} = \frac{0.2}{\Omega_m h} \left( \frac{100}{g_{dec}} \right)^{4/3} \text{ Mpc} = \quad (49)$$

$$0.065 h^{-1} \text{ Mpc} \left( \frac{\Omega_m}{0.3} \right)^{1/3} \left( \frac{h}{0.65} \right)^{5/3} \left( \frac{1 \text{ keV}}{M_{DM}} \right)^{4/3},$$

where  $g_{dec}$  is the effective number of particle degrees of freedom at the period of particles decoupling (Bardeen et al. 1986). Variations of the spectral moments and  $q_0$  with the mass of DM particle obtained by integration of the power spectrum with the exponential cutoff

$$p(x) \propto x T^2(x) \exp(-x R_f - (x R_f)^2), \quad (50)$$

$$R_f = R_{fw} k_0 = 0.2 \left( \frac{\Omega_m h^2 \text{ keV}}{M_{DM}} \right)^{4/3},$$

are plotted in Fig. 10 for CDM and WDM models.

As is seen from this Fig. our estimates

$$q_0 \approx (2 - 0.8) \cdot 10^{-2}, \quad m_0 \approx 0.1 - 0.4, \quad (51)$$

$$M_{DM} \approx (0.6 - 2) \text{ keV}$$

are close to estimates of Narayanan et al. (2000) and Barkana, Haiman & Ostriker (2001).

There are plenty of possible candidates for the WDM particles with the mass  $\sim 1 \text{ keV}$ . They are, for example, the sterile neutrinos, majorons and even shadow particles. Detailed review of possible candidates can be found in Sommer-Larsen & Dolgov (2001) and Dolgov (2002).

However, the observational estimates are based on the spectral moments and their interpretation as a mass of the



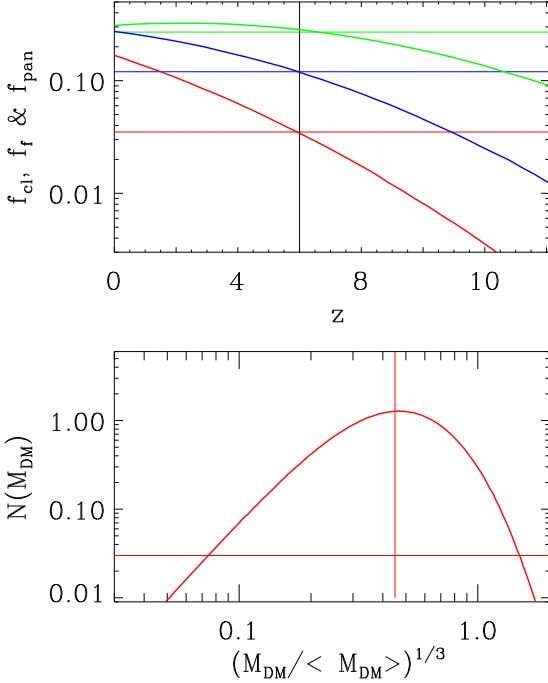


**Figure 11.** Top panel: redshift variations of the DM fraction accumulated by high density clouds, filaments and pancakes (red, green and blue lines), respectively at  $q_0 = 10^{-2}$ . Bottom panel: the expected mass function of the DM clouds at  $z = 6$  and  $q_0 = 10^{-2}$ .

DM particles seems to be natural but not unique. In particular, this result does not forbid the existence of multicomponent dark matter with the same spectral moments  $m_{-2}$  and  $m_0$ . Also the shape of initial power spectrum can be different from the one used here.

## 7.6 Reheating of the Universe

Recent observations of high redshift quasars with  $z \geq 5$  (Djorgovski et al. 2001; Becker et al. 2001; Pentericci et al. 2001; Fan et al. 2001) demonstrate clear evidences in favor of the reionization of the Universe at redshifts  $z \sim 6$  when the volume averaged fraction of neutral hydrogen is found to be  $f_H \geq 10^{-3}$  and the photoionization rate  $\Gamma_\gamma \sim (0.2 - 0.8) \cdot 10^{-13} s^{-1}$ . These data coincide with those expected at the end of the reionization epoch which probably takes place at  $z \sim 6$ . Extrapolation of the mean separation of absorbers discussed in Sec. 6.4 is consistent with these conclusions.

These results can be compared with expectations of the Zel'dovich approximation (DD02) for  $q_0 = 10^{-2}$ . The potential of this approach is limited especially with respect to the description of nonlinear stages of structure formation and, so, it cannot substitute the high resolution numerical simulations. However, it describes quite well many observed and simulated statistical characteristics of the structure such as the redshift distribution of absorbers and evolution of their DM column density. This approach is not influenced by the box size, number of points and other limitations of numerical simulations and successfully augments them.

This approach allows to estimate the fractions of DM component accumulated by high density clouds,  $f_{cl}$ , fila-

ments,  $f_f$ , and pancakes,  $f_{pan}$ , at different redshifts. These functions plotted in Fig. 11 for  $q_0 = 10^{-2}$  show that at  $z \sim 6$  only  $\sim 3.5\%$  of the matter is condensed within the high density clouds which can be associated with luminous objects. This value can be increased up to  $\sim 5 - 6\%$  for more correct description of the cloud collapse. At the same redshifts,  $\sim 27\%$  and  $\sim 12\%$  of the matter can be already accumulated by pancakes and filaments, respectively.

The Zel'dovich approximation allows also to estimate the mass function of all structure elements (DD02) at different redshifts. For  $q_0 = 10^{-2}$  and at  $z \sim 6$ , this function is plotted in Fig. 11. For these  $q_0$  and  $z$ , the mean DM mass of structure elements is expected to be  $\sim 10^{12} M_\odot$  and the main mass is concentrated within clouds with  $M_{DM} \sim 0.1 \langle M_{DM} \rangle$ . As is seen from Fig. 11, majority of the clouds are situated between  $10^{-3} \langle M_{DM} \rangle$  and  $10 \langle M_{DM} \rangle$ . The formation of low mass clouds with  $M_{DM} \leq 10^9 M_\odot$  is suppressed due to strong correlation of the initial density and velocity fields at scales  $\leq l_p \sim 0.3 h^{-1}$  Mpc (48). However, the numerous low mass satellites of large central galaxies can be formed in the course of disruption of massive collapsed clouds at the stage of their compression into thin pancake-like objects (Doroshkevich 1980; Vishniac 1983). The minimal mass of such satellites was estimated in Barkana, Haiman & Ostriker (2001).

This means that the investigation of absorbers observed at high redshifts must be followed by the study of properties of dwarf *isolated* galaxies and discrimination between such galaxies and dwarf satellites of more massive galaxies. It seems to be a perspective way to discriminate between models with the initial power spectrum (50) and more complicated ones and, in particular, between models with one and several types of DM particles.

These preliminary inferences can be tested with further observations of high redshift objects and a richer sample of observed absorbers. Such sample will allow to improve the description and to obtain more detailed and reliable information about the structure evolution, physical processes at high redshifts and properties of the initial power spectrum.

## Acknowledgments

AGD is grateful to Dr. S. Cristiani and Dr. T.S.Kim for the permission to use the unpublished observational data. This paper was supported in part by Denmark's Grundforskningsfond through its support for an establishment of Theoretical Astrophysics Center and by the Polish State Committee for Scientific Research grant Nr. 2-P03D-014-17. AGD also wish to acknowledge support from the Center of Cosmo-Particle Physics, Moscow.

## REFERENCES

- Bahcall J.N. et al., 1993, ApJS., 87, 1.
- Bahcall J.N. et al., 1996, ApJ., 457, 19.
- Bardeen J.M., Bond J.R., Kaiser N., Szalay A., 1986, ApJ., **304**, 15 (BBKS)
- Barkana R., Haiman Z., Ostriker J.P., 2001, ApJ., 558, 482
- Bergeron J., Cristiani S., & Shaver P.A., 1992, A&A, **257**, 417
- Bi H., & Davidsen A.F., 1997, ApJ., **479**, 523
- Black J.H., 1981, MNRAS, **197**, 553
- Becker R.H. et al. 2001, AJ., 122, 2850

- Bode P., Ostriker J.P. & Turok N., 2001, *ApJ.*, **556**, 93
- Colin P., Avila-Reese V., & Valenzuela O., 2001, *ApJ.*, **542**, 622
- Cook A.J., Espey B. & Carswell R.F., 1997, *MNRAS*, **284**, 552
- Cristiani S., D'Odorico V., 2000, *AJ*, **120**, 1648
- Croft R.A.C. et al., 2000, *ApJ.*, subm. astro-ph/0012324
- Davé R., Hernquist L., Katz N., Weinberg D.H., 1999, *ApJ.*, **511**, 521,
- Demiański M. & Doroshkevich A., 1999, *MNRAS.*, **306**, 779, (DD99).
- Demiański M. & Doroshkevich A., 2002, *MNRAS.*, submit., astro-ph/0206282 (DD02)
- Demiański M., Doroshkevich A.G., & Turchaninov V.I., 2001, *MNRAS*, **318**, 1177, (Paper I)
- Demiański M., Doroshkevich A.G., & Turchaninov V.I., 2001, *MNRAS*, **318**, 1189, (Paper II)
- Demiański M., Doroshkevich A.G., Müller V., & Turchaninov V.I., 2000, *MNRAS*, **318**, 665
- Djorgovski S.G., Castro S., Stern D., Mahabal A.A., 2001, *ApJ.*, **560**, L5
- Dolgov A., 2002, *Phys.Rep.*, in press, hep-ph/0202122
- Doroshkevich, A.G., 1980, *SvA.*, **24**, 152
- Doroshkevich, A.G., Tucker, D.L. & Allam S., 2002, *MNRAS.*, submit., astro-ph/0206301
- Efstathiou G. et al., 2001, astro-ph/0109152
- Fan X. et al., 2001, astro-ph/0111184, *ApJ.*, in press
- Giallongo E., Cristiani S., Fontana A., & Trevese D., 1993, *ApJ.*, **416**, 137
- Hu E.M., Tae-Sun K., Cowie L., & Songaila A., 1995, *AJ*, **110**, 1526
- Ikeuchi S., Ostriker J.P., 1986, *ApJ.*, **301**, 522.
- Jannuzi B.T. et al. *ApJS*. 1998, **118**, 1
- Jacobsen P., et al. 1994, *Nature*, **370**, 35
- Khare P. et al., 1997, *MNRAS*, **285**, 167.
- Kim T.S., Cristiani S., & D'Odorico S., 2002, *A&A*, in press, astro-ph/0201204
- Kim T.S., Carswell R.F., Cristiani S., D'Odorico S. & Giallongo E., 2002, *MNRAS*, in press, astro-ph/0205237
- Kirkman D., & Tytler D., 1997, *ApJ.*, **484**, 672.
- Kulkarni V.P. et al., 1996, *MNRAS*, **279**, 197
- Lanzetta K.M., Bowen D.V., Tytler D., & Webb J.K., 1995, *ApJ.*, **442**, 538.
- Le Brune V., Bergeron J., & Boisse P., 1996, *A&A*, **306**, 691
- Lu L., Sargent W.L.W., Womble D.S., Takada-Hidai M., 1996, *ApJ.*, **472**, 509
- McGill C., 1990, *MNRAS*, **242**, 544
- Narayanan V. et al., 2000, *ApJ.*, **543**, L103
- Oort J.H., 1981, *Astr.Astrophys.*, **94**, 359.
- Oort J.H., 1984, *Astr.Astrophys.*, **139**, 211.
- Pentericci L. et al., 2001, astro-ph/0112075
- Penton S.V., Stocke J.T., & Shull J.M., 2002, *ApJ.*, **565**, 720
- Rauch M., 1998, *Ann.Rev.Astr.Astrophys.*, **36**, 267
- Rodriguez-Pascual P.M., de la Fuente A., 1995, *ApJ.*, **448**, 575.
- Sargent, W.L.W., Young, P.J., Boksenberg, A. & Tytler, D., 1980, *Ap.J.Suppl.*, **42**, 41
- Shandarin S., Zel'dovich Ya.B., 1989, *Rev.Mod.Phys.*, **61**, 185
- Shandarin S. et al., 1995, *Phys.Rev.Let.*, **75**, 7
- Shectman S.A. et al., 1996, *ApJ.*, **470**, 172.
- Sommer-Larsen J. & Dolgov A., 2001, *ApJ.*, **551**, 608
- Songaila A., 1998, *AJ.*, **115**, 2184
- Stoughton C. et al., 2001, *AJ.*, **123**, 485
- Theuns T., Zaroubi S., & Kim T.-S., *Proceedings XVII IAP colloquium*, in press, astro-ph/0110552
- Tytler D., 1995, in Meylan J., ed., *QSO Absorption Lines*, p. 289.
- Vishniac E.T., 1983, *ApJ.*, **274**, 152
- Weinberg D.H., Burles S., Croft R.A.C., et al., 1998, in "Evolution of Large Scale Structure: From Recombination to Garching", eds. A.J. Banday, R.K. Sheth, L.N. Da Costa, p. 346
- Zel'dovich Ya.B., 1970, *Astrophysica*, **5**, 20
- Zeng W., Davidsen A.F., & Kriss G.A., 1998, *AJ*, **115**, 391
- Zhang Yu., Meiksin A., Anninos P., Norman M.L., 1998, *ApJ.*, **495**, 63